A hysteretic hydraulic constitutive model for unsaturated soils and application to capillary barrier systems

Author 1

- Riccardo Scarfone, Geotechnical Engineer, previously Marie Sklodowska-Curie Early Stage Researcher
- Geotechnical Consulting Group LLP, London, United kingdom; James Watt School of Engineering, University of Glasgow, Glasgow, United Kingdom.
- https://orcid.org/0000-0003-0268-9537
- r.scarfone@gcg.co.uk; riccardo.scarfone@glasgow.ac.uk

Author 2*

- Simon J. Wheeler*, Cormack Professor of Civil Engineering
- James Watt School of Engineering, University of Glasgow, Glasgow, United Kingdom
- https://orcid.org/0000-0003-1493-2434
- Simon.Wheeler@glasgow.ac.uk

***Corresponding author.**

Author 3

- Marti Lloret-Cabot, Assistant Professor
- Department of Engineering, Durham University, Durham, United Kingdom
- https://orcid.org/0000-0002-7746-8213
- marti.lloret-cabot@durham.ac.uk

Article type: Research paper

Number of words: 11652

Number of figures: 15

Number of tables: 4

Abstract

Unsaturated soils exhibit water retention hysteresis, with different water retention behaviour during drying and wetting paths. Water retention hysteresis has often been modelled using expressions for the main drying and main wetting water retention curves that are unsatisfactory at low values of degree of saturation. In addition, the effect of retention hysteresis on the unsaturated hydraulic conductivity behaviour has typically not been explicitly considered. This paper presents a new hysteretic hydraulic constitutive model for the water retention and hydraulic conductivity behaviour of unsaturated soils, which is effective and easy to apply. The model includes: i) main wetting and main drying water retention curves modelled with a modified version of the van Genuchten model, improved at low degree of saturation; ii) hysteretic scanning water retention curves modelled using a bounding surface approach; iii) the effect of hydraulic hysteresis on a SHCC model improved at low degree of saturation and including the effect of liquid film conductivity. The new hysteretic hydraulic model is then validated against experimental data. After implementation in the finite element software Code_Bright, the new hydraulic constitutive model is applied in a numerical study of the impact of hydraulic hysteresis on the behaviour of capillary barrier systems (CBSs). Water retention hysteresis, which has typically been neglected in the modelling of the hydraulic behaviour of CBSs, is shown to have a significant impact on: i) movement and redistribution of water within the finer layer of a CBS; ii) the phenomenon of water breakthrough across the interface between the finer and coarser layers of a CBS and the subsequent restoration of the CBS after infiltration at the ground surface ceases; iii) the prediction of evaporation from a CBS into the atmosphere.

Keywords

Unsaturated soils; Water retention hysteresis; Hydraulic conductivity; Capillary barrier systems; Numerical modelling.

Research data for this article

All data presented in this article are available in a repository online in accordance with funder data retention policies. The online repository is the institutional repository “Enlighten” of the University of Glasgow and the data can be accessed using the following DOI: http://dx.doi.org/10.5525/gla.researchdata.1073.

1. Introduction

The hydraulic behaviour of unsaturated soils is represented by the soil water retention curve (SWRC), i.e. the relationship between degree of liquid saturation S_l and suction s, and the soil hydraulic conductivity curve (SHCC), i.e. the relationship between hydraulic conductivity k_l and either degree of saturation or suction.

For a given soil, the water retention curve is not unique, with different retention behaviour during drying and wetting paths (Haines, 1930); an effect known as retention hysteresis. In addition, water retention behaviour is affected by changes of void ratio of the soil (e.g. Gallipoli et al., 2003). This paper focuses on the inclusion of retention hysteresis within non-deformable unsaturated soils (i.e. the influence of changes of void ratio is not included).

In terms of retention behaviour, two limit curves can be identified: the "main drying curve", representing a drying process which starts from a saturated condition, and the "main wetting curve", representing a wetting process which starts from a dry condition. "Scanning curves" lie between the main drying curve and main wetting curve, and these represent paths followed after reversals between drying and wetting at intermediate values of degree of saturation. Some authors (e.g. Likos et al., 2013) distinguish between a "primary drying curve" (followed during drying from a saturated condition) and a "main drying curve" (followed during drying from the end point of the main wetting curve), however it is argued later in this paper that this distinction is unnecessary.

The main cause of retention hysteresis is the “ink-bottle effect” (Haines, 1930), caused by the fact that the value of suction at which a void fills with water during wetting is associated with the radius of the void, whereas the value of suction at which the same void empties of water during drying is associated with the smaller radius of a narrow throat giving entry of air to the void. Other causes of retention hysteresis include differences of contact angle during drying and wetting (Klausner, 2012).

Several hysteretic SWRC models have been proposed. These hysteretic SWRC models can be divided into two groups: the conceptual (or physically based) models and the empirical models. The conceptual models assume that the soil is made of a domain of pores which are either filled or empty of water and two different values of suction are associated to each pore: one which causes water-filling of the pore and one which causes water-emptying of the pore. A detailed review of the conceptual hysteretic SWRC models is given by Pham et al. (2005). The empirical hysteretic SWRC models assume mathematical forms for the main drying curve, main wetting curve, scanning drying curves and scanning wetting curves and then the values of relevant soil constants in the mathematical expressions are selected to fit the predicted curves to experimentally observed behaviour. In recent years, empirical hysteretic SWRC models have been more widely used than physically based models, in particular when coupled with mechanical models for unsaturated soils.

In some empirical hysteretic SWRC models, in particular those which relate retention hysteresis and mechanical behaviour, once the main wetting and main drying curves were defined, the scanning curves were simply approximated by straight lines in a linear plot (Hanks et al., 1969) or in a semi-logarithmic plot (Wheeler et al., 2003; Khalili et al., 2008; Nuth and Laloui, 2008). Other empirical hysteretic SWRC models related the shape of the scanning curves to the shape of the corresponding main drying or main wetting curve (Dane and Wierenga, 1975; Jaynes, 1984; Scott et al., 1983; Kool and Parker, 1987; Parker and Lenhard, 1987). Among these, the model proposed by Kool and Parker (1987) is probably the most widely used because it has been implemented in commercial numerical codes, e.g. UNSAT-H (Fayer, 2000). According to this model, a scanning curve is modelled as a scaled version of the corresponding main curve passing through the last reversal point (e.g. a scanning drying curve is a scaled version of the main drying curve). This model may however predict unrealistic results when used to model cyclic variations of suction, leading to an artificial "pumping effect" (Klute and Heermann, 1974) that can result in scanning curves falling outside the main curves. In order to solve this drawback, Parker and Lenhard (1987) proposed a modification to the model. This consisted of enforcing that scanning wetting-drying loops must be closed. Although this model solved the artificial pumping effect of the Kool and Parker model, it has two drawbacks: (i) the prediction of wetting-drying loops which are always closed may be unrealistic; (ii) when implemented in a numerical code, the model may require high memory capacity because all the reversal points at all the positions of the numerical model must be saved.

More recently, various empirical SWRC models based on "bounding surface" concepts have been proposed (Li, 2005; Pedroso et al., 2009; Zhou et al., 2012; Gallipoli et al., 2015). In these bounding surface hysteretic SWRC models, the slope of a scanning curve is related to the slope of the corresponding main curve at the same value of degree of saturation.

All existing empirical hysteretic SWRC models assume conventional empirical (non-hysteretic) SWRC expressions to describe the main drying curve and the main wetting curve, such as those proposed by Brooks and Corey (1964) or Van Genuchten (1980).

The empirical hysteretic SWRC models are also typically used in conjunction with a conventional SHCC expression, such as Mualem (1976), for the hydraulic conductivity behaviour. Although the conventional SWRC and SHCC expressions are able to represent well the retention and hydraulic conductivity behaviour of unsaturated soils at medium and high values of degree of saturation, they are unreliable at very low values of degree of saturation, in the pendular condition, when the soil pores all contain air and the liquid water present in the soil is only in the forms of meniscus water bridges around particle contacts and thin liquid films around each soil particle (Scarfone et al., 2020). In addition, little consideration has been given to whether combination of a given hysteretic SWRC model with a conventional SHCC expression, such as Mualem (1976), results in appropriate representation of any hysteresis in the hydraulic conductivity behaviour.

Recently, Rudiyanto et al. (2015) proposed a complete hydraulic model for unsaturated soils accounting for retention hysteresis and incorporating improved modelling of SWRC and SHCC at low degree of saturation. Although this model represents an interesting contribution towards a complete hydraulic model for unsaturated soils, improved at low degree of saturation and including retention hysteresis, it is affected by some weaknesses: (i) the SHCC model is not fully predictive; (ii) it employs the hysteretic SWRC model proposed by Parker and Lenhard (1987), which is affected by weaknesses discussed above. For this reason, the first aim of this paper is to present a new hysteretic hydraulic constitutive model for unsaturated soils, improved at low degree of saturation, including the SHCC and easy to apply.

Accurate modelling of the hysteretic hydraulic behaviour of unsaturated soils can find applications in a wide variety of problems in geotechnical engineering. One of these is numerical modelling of the hydraulic behaviour of capillary barrier systems, which are typically subjected to multiple cycles of rain (i.e. wetting) and evapotranspiration (i.e. drying).

Capillary barrier systems (CBSs) are geotechnical structures made of an upper finer layer (F.L.) overlying a lower coarser layer (C.L.), placed over the ground with the aim of preventing the percolation of water into the underlying soil (Stormont and Anderson, 1999). The coarser layer is typically at very low degree of saturation and, consequently, the corresponding unsaturated hydraulic conductivity may be several orders of magnitude lower than that of the finer layer. Thus, prior to significant water breakthrough into the coarser layer, rainwater is stored in the finer layer whereas the coarser layer acts as an almost impermeable barrier. This water can then be removed by evapotranspiration (Khire et al., 2000) and, if the barrier is sloped, by lateral drainage (Ross, 1990). The barrier fails when the amount of water stored in the F.L. is so high that the suction at the interface between F.L. and C.L. reduces to the “bulk water-continuity value” of the coarser layer, at which the hydraulic conductivity of the C.L. starts increasing significantly (Scarfone et al., 2020). At this point, water breakthrough occurs from the F.L. to the C.L., and eventually into the underlying soil.

Surprisingly, although water retention hysteresis is expected to be relevant in the modelling of the behaviour of CBSs, since they are subjected to multiple cycles of rain and evapotranspiration, only very few authors (e.g. Zhang et al., 2009) considered the role of water retention hysteresis in the numerical modelling of CBSs.

This paper initially presents a new hysteretic hydraulic constitutive model, including retention behaviour and hydraulic conductivity behaviour, improved at low degree of saturation and obtained using a bounding surface approach. This hysteretic hydraulic constitutive model is then validated against experimental data. Finally, the new model is employed in a numerical study of the hydraulic behaviour of a CBS by means of the finite element software Code_Bright (Olivella et al., 1996).

2. Hysteretic hydraulic constitutive model

In this section, a new hysteretic hydraulic constitutive model for unsaturated soils improved at low degree of saturation is presented. The model involves the definition of the following elements:

- main drying and main wetting SWRCs;
- scanning retention curves;
- SHCCs, including the effect of hydraulic hysteresis.

The model assumes that the soil is incompressible and it is intended for application to relatively coarse-grained soils, because the effect of deformation due to changes in suction, mainly relevant to fine-grained soils, is not considered.

2.1 Main drying and main wetting SWRCs

The main drying curve and the main wetting curve are each represented by a modified version of the conventional van Genuchten (1980) expression. The modification was proposed by Fayer and Simmons (1995), to provide improved modelling at low values of degree of saturation.

In the conventional van Genuchten expression, the degree of saturation S_l is given by:

$$S_l = S_{lr} + \left(S_{ls} - S_{lr}\right) \cdot S_{le}$$

(1)

where S_{lr} is the residual degree of saturation, S_{ls} is the maximum value of degree of saturation (both S_{lr} and S_{ls} are soil constants) and S_{le} is the effective degree of saturation (with a value between 0 and 1), which varies with suction according to:

$$S_{le} = \left[1 + \left(\frac{s}{P_0}\right)^n\right]^{-m}$$

(2)

where P_0, n and m are parameters of the model (soil constants). Parameters m and n are often correlated as m=1-1/n (van Genuchten, 1980). Equations 1 and 2 mean that the conventional van Genuchten SWRC model predicts that S_l varies from a maximum value S_{ls} at s=0 to a minimum value S_{lr} as s tends to infinity.

The conventional van Genuchten (VG) model of Equations 1 and 2 cannot accurately represent the SWRC at low values of S_l. As shown in Figure 1, the VG model predicts that S_l tends asymptotically to a minimum value S_{lr} as s tends to infinity (typically non-zero values of S_{lr} are employed in the VG model, to produce a reasonable fit to experimental data at intermediate values of S_l). In contrast, experimental results at very low values of S_l (Campbell and Shiowaza, 1992), supported by thermodynamic considerations (Richards, 1965), show that the value of S_l reduces to zero at a finite value of suction of approximately s_{dry}=1GPa, regardless of the type of soil.

In particular, experimental results (e.g. Campbell and Shiowaza, 1992) show that at low values of degree of saturation the SWRC decreases approximately linearly with the logarithm of suction and Fayer and Simmons (1995) proposed a modified version of the VG model to capture this behaviour and hence to extend the use of the model to very low values of S_l . In the modified van Genuchten (modVG) SWRC model of Fayer and Simmons (1995)[1], Equation 1 is replaced by:

$$S_l = \xi \cdot \ln\left(\frac{s_{dry}}{s}\right) + \left(S_{ls} - \xi \cdot \ln\left(\frac{s_{dry}}{s}\right)\right) \cdot S_{le}$$

(3)

where ξ is a fitting parameter, s_{dry} is the suction at oven dryness, i.e. s_{dry}=1GPa, and the effective degree of saturation S_{le} is still given by Equation 2. A qualitative comparison between the performance of the VG and modVG models is shown in Figure 1. Fayer and Simmons (1995) showed that Equation 3 could also be used to produce a modified version (modBC) of the conventional Brooks and Corey (1964) SWRC model and Khlosi et al. (2006) used the same approach to produce a modified version (modK) of the conventional Kosugi (1996) SWRC model.

In this paper, the modVG model of Equations 2 and 3 is used to represent the main drying SWRC and the main wetting SWRC. Different values of the soil parameter P_0 (see Equation 2) are required for the main drying curve and the main wetting curve, with $P_{0d}>P_{0w}$.

In using the modVG model within numerical analyses it is recommended that the maximum value of degree of saturation S_{ls} in Equation 3 is taken as S_{ls}=1 for both the main drying curve and the main wetting curve. Laboratory wetting tests may appear to show that S_{ls} should be less than 1 for a main wetting SWRC, due to the influence of air entrapment during wetting (Stonestrom and Rubin, 1989). However, Scarfone (2020)

[1] In the original paper of Fayer and Simmons (1995), the modVG model is expressed rather differently to Equation 3 and in terms of volumetric water content θ_l, rather than degree of saturation S_l. The parameter ξ in Equation 3 is related to the parameter β in the original expression of Fayer and Simmons by the following relationship: $\xi=(S_{ls}\cdot\theta_a)/(\theta_s \ln(\beta h_m))$, where θ_a, θ_s, β and h_m are parameters in the original Fayer and Simmons expression ($h_m=s_{dry}/\gamma_l$, where γ_l is the unit weight of water).

shows that, once air trapping occurs, the apparent SWRC measured in a wetting test in the laboratory is not the same as the true SWRC (unless the laboratory test is performed exceptionally slowly) because the gas pressure in the trapped air is greater than the externally applied gas pressure. The true main wetting SWRC, of S_l plotted against the true internal suction (the difference between the pore liquid pressure and the gas pressure within the trapped air), reaches full saturation at a positive value of suction (the air exclusion point). Hence, it is appropriate to assume S_{ls} = 1 when using the VG or modVG model to describe the true main wetting SWRC. In contrast, the apparent main wetting SWRC measured in a laboratory test (with S_l plotted against the externally applied suction) is not simply a representation of the soil behaviour, as it also depends upon many aspects of the wetting test conditions. Scarfone (2020) shows that the only correct way to represent the occurrence and influence of air trapping during wetting within numerical modelling is to use the true SWRC in combination with a gas conductivity expression that goes to zero when the gas phase becomes discontinuous. If the true main wetting curve is used (with S_{ls}=1), there is no distinction between the “main drying curve” and the “primary drying curve”, as described earlier. Throughout the remainder of this paper, the term “main drying curve” is preferred to “primary drying curve” (for consistency with the terminology of “main wetting curve”), except in discussing experimental data where it is clear that wetting was performed too fast to measure a true main wetting curve and hence there was a need to distinguish between measured drying curves corresponding to primary drying and main drying.

At very low values of S_l, in the pendular condition, where liquid water is present only in the forms of meniscus water bridges and liquid films, experimental results show that the water retention behaviour is non-hysteretic (Schelle et al., 2013). As a consequence, the value of the parameter ξ in Equation 3 would be expected to take the same value for the main drying SWRC and the main wetting SWRC (ξ_d=ξ_w). In addition, with S_{lsd}= S_{lsw} and ξ_d=ξ_w, there should theoretically be a requirement that the value of the parameter n in Equation 2 should take the same value for the main drying SWRC and the main wetting SWRC (n_d=n_w and hence m_d=m_w), otherwise the main wetting curve would lie above the main drying curve at extreme values of s, which is impossible (this problem would occur at very high values of s for n_d>n_w and at very low values of s for n_d<n_w). In practice, however, it is probably acceptable to have different values of n for the main drying SWRC and the main wetting SWRC, if this provides a better match to experimental SWRCs, because the main wetting curve will typically be predicted to lie above the main drying curve only at very extreme values of s, where the values of S_{le} predicted by Equation 2 are so close to zero or 1 that the main drying curve and the main wetting curve are indistinguishable.

Figure 2 shows typical main drying and main wetting SWRCs predicted by the modVG model (Equations 2 and 3), with P_{0d}>P_{0w}, S_{lsd}=S_{lsw}=1 and ξ_d=ξ_w, but with n_d>n_w.

2.2 Scanning retention curves

Scanning retention curves are modelled using a bounding surface approach proposed by Gallipoli et al. (2015), in which the gradient of a scanning drying curve $(\mathrm{d}S_{le}/\mathrm{d}\ln s)_d$ and the gradient of a scanning wetting curve $(\mathrm{d}S_{le}/\mathrm{d}\ln s)_w$ (expressed in a semi-logarithmic plot of effective degree of saturation S_{le} against the logarithm of suction $\ln s$) at a general point A (see Figure 3) are related to the corresponding gradient of the main drying curve $(\mathrm{d}S_{le}/\mathrm{d}\ln s)_{Md}$ or main wetting curve $(\mathrm{d}S_{le}/\mathrm{d}\ln s)_{Mw}$ respectively by:

$$\left(\frac{\mathrm{d}S_{le}}{\mathrm{d}\ln s}\right)_d = \left(\frac{s}{s_d}\right)^{\gamma_d}\left(\frac{\mathrm{d}S_{le}}{\mathrm{d}\ln s_d}\right)_{Md}$$

(4a)

$$\left(\frac{\mathrm{d}S_{le}}{\mathrm{d}\ln s}\right)_w = \left(\frac{s_w}{s}\right)^{\gamma_w}\left(\frac{\mathrm{d}S_{le}}{\mathrm{d}\ln s_w}\right)_{Mw}$$

(4b)

s_d and s_w are the image values of suction, namely the suction values corresponding to the horizontal projection (at the same effective degree of saturation S_{le}) of the current point A (s,S_{le}) onto the main drying curve or the main wetting curve at point B (see Figure 3). $(\mathrm{d}S_{le}/\mathrm{d}\ln s)_{Md}$ and $(\mathrm{d}S_{le}/\mathrm{d}\ln s)_{Mw}$ are respectively the gradients of the main drying curve and the main wetting curve (in the same semi-logarithmic plot of S_{le} against ln$s$) at their image points B (see Figure 3). The terms γ_d and γ_w are parameters of the model (soil constants) for the scanning drying curve and scanning wetting curve respectively and they always assume positive values. The closer is the current value of suction s to its image value, s_d or s_w, the closer is the gradient of the scanning curve to the gradient of its corresponding main drying or main wetting curve. The main curve thus represents an asymptotic limit for the corresponding scanning curve.

The parameters γ_d and γ_w control the shape of the scanning curves, as shown in Figure 3, where the scanning curve from A shown by the chain-dotted line is for a higher value of γ_d or γ_w than the scanning curve from A shown by the continuous line. As the value of γ_d or γ_w increases, the variation of the gradient of the scanning curve becomes sharper. At the upper limit, i.e. $\gamma_d \rightarrow \infty$ or $\gamma_w \rightarrow \infty$, the scanning curve is horizontal in the S_{le}:ln$s$ plot until reaching the corresponding main curve, at which point, the gradient of the scanning curve changes sharply and the scanning curve follows the corresponding main curve. In contrast with other models in which scanning curves are modelled as scaled versions of the corresponding main curves (e.g. Kool and Parker, 1987; Parker and Lenhard, 1987), the introduction of γ_d and γ_w as two additional parameters allows a greater degree of freedom in representing the scanning curves, although the parameter values must be determined for each soil.

The modVG expression of Equation 2, defining the main drying SWRC and the main wetting SWRC, can be inverted to give expressions for the image values of suction s_d and s_w in terms of the current effective degree of saturation S_{le}:

$$s_d = P_{0d} \cdot \left(S_{le}{}^{-1/m_d} - 1 \right)^{1/n_d}$$

(5a)

$$s_w = P_{0w} \cdot \left(S_{le}{}^{-1/m_w} - 1 \right)^{1/n_w}$$

(5b)

where P_{0d}, n_d and m_d are the parameters of the modVG model for the main drying SWRC and P_{0w}, n_w and m_w are the parameters of the modVG model for the main wetting SWRC.

From Equations 4a and 4b, in combination with Equations 5a and 5b, and after some algebraic manipulation (see Scarfone, 2020), the following closed-form relationships can be obtained, describing the variation of effective degree of saturation S_{le} along a scanning drying curve or a scanning wetting curve:

$$S_{le,d} = \left\{ 1 + \left[\frac{\left(s^{\gamma_d} - A_d \right)^{1/\gamma_d}}{P_{0d}} \right]^{n_d} \right\}^{-m_d}$$

(6a)

$$S_{le,w} = \left\{ 1 + \left[\frac{\left(s^{-\gamma_w} - A_w \right)^{-1/\gamma_w}}{P_{0w}} \right]^{n_w} \right\}^{-m_w}$$

(6b)

The integration constants A_d and A_w are calculated by imposing the condition that the scanning curve passes through the reversal point (s_0,S_{le0}):

$$A_d = s_0^{\gamma_d} - \left[P_{0d} \cdot \left(S_{le0}^{-1/m_d} - 1 \right)^{1/n_d} \right]^{\gamma_d}$$

(7a)

$$A_w = s_0^{-\gamma_w} - \left[P_{0w} \cdot \left(S_{le0}^{-1/m_w} - 1 \right)^{1/n_w} \right]^{-\gamma_w}$$

(7b)

where S_{le0} is the effective degree of saturation at the reversal point, which can be obtained from the actual degree of saturation at the reversal point S_{l0} as:

$$S_{le0} = \frac{S_{l0} - \xi_d \ln\left(\frac{s_{dry}}{s} \right)}{S_{ls,d} - \xi_d \ln\left(\frac{s_{dry}}{s} \right)} \qquad \text{for drying}$$

(8a)

$$S_{le0} = \frac{S_{l0} - \xi_w \ln\left(\frac{s_{dry}}{s} \right)}{S_{ls,w} - \xi_w \ln\left(\frac{s_{dry}}{s} \right)} \qquad \text{for wetting}$$

(8b)

where $S_{ls,d}$ and ξ_d are the parameters of the modVG model for the main drying SWRC and $S_{ls,w}$ and ξ_w are the parameters of the modVG model for the main wetting SWRC.

Equation 3, giving the general relationship between degree of saturation S_l and effective degree of saturation S_{le} in the modVG model, means that the variation of S_l along a scanning drying curve ($S_{l,d}$) or a scanning wetting curve ($S_{l,w}$) is given by:

$$S_{l,d} = \xi_d \ln\left(\frac{s_{dry}}{s} \right) + \left[S_{ls,d} - \xi_d \ln\left(\frac{s_{dry}}{s} \right) \right] \cdot S_{le,d}$$

(9a)

$$S_{l,w} = \xi_w \ln\left(\frac{s_{dry}}{s}\right) + \left[S_{ls,w} - \xi_w \ln\left(\frac{s_{dry}}{s}\right)\right] \cdot S_{le,w}$$

(9b)

Equations 9a and 9b, in combination with Equations 6a, 6b, 7a, 7b, 8a and 8b, form a simple but effective method to include water retention hysteresis in the modVG SWRC model.

Scarfone (2020) also examined a slightly different hysteretic version of the modVG SWRC model, where Equations 4a and 4b were replaced with alternative expressions, where effective degree of saturation S_{le} was replaced by degree of saturation S_l. Scarfone (2020) showed that the predictions of the two different versions of hysteretic modVG model were indistinguishable, but the version presented here (based on Equations 4a and 4b) has two advantages. Firstly, it has a slightly stronger physical justification, because one of the most important causes of retention hysteresis is the "ink-bottle effect" described earlier, which is linked to the bulk water component of the liquid water present in an unsaturated soil, and the volume of this bulk water is implicitly associated with the effective degree of saturation S_{le} in the modVG model (whereas the remainder of the degree of saturation S_l is implicitly associated with the volume of water within meniscus water bridges and liquid films). Secondly, the version of hysteretic modVG model based on Equations 4a and 4b is mathematically much simpler than the alternative version, and much less computationally demanding when implemented within a finite element code, because, with the modVG model, the expression for S_{le} (see Equation 2) can be inverted to provide closed form expressions for the image values of suction s_d and s_w in terms of the current effective degree of saturation S_{le} (see Equations 5a and 5b), whereas the expression for S_l (see Equations 3 and 2) cannot be inverted.

Scarfone (2020) showed that the hysteretic approach represented by Equations 4a and 4b (Gallipoli et al., 2015) is also suitable for developing hysteretic versions of other existing (non-hysteretic) SWRC models, provided that the existing model involves an expression for effective degree of saturation S_{le} that can be inverted to give suction s as an explicit function of S_{le}. He demonstrated this by presenting hysteretic versions of the modified Brooks and Corey (modBC) and modified Kosugi (modK) SWRC models described earlier.

2.3 SHCC model

Scarfone et al. (2020) recently showed that the conventional Mualem (1976) SHCC model used in conjunction with the van Genuchten SWRC model is unable to describe accurately the hydraulic conductivity of unsaturated soils at low values of degree of saturation and they proposed a new SHCC model to address this problem. According to this new SHCC model, known as the Modified Mualem plus Liquid Film (modM+LF) model, following the general approach adopted by Peters (2013), the hydraulic conductivity k_l can be split into two components:

$$k_l = k_l^{Bulk} + k_l^{Film} \tag{10}$$

where k_l^{Bulk} is the component of hydraulic conductivity related to liquid flow occurring through the bulk water whereas k_l^{Film} is the component of hydraulic conductivity related to liquid flow occurring within thin liquid films covering the surfaces of soil particles, connected by meniscus water bridges at inter-particle contacts. At medium and high values of degree of saturation, the hydraulic conductivity is controlled by the bulk water component k_l^{Bulk} whereas, at very low values of degree of saturation, when bulk water is no longer present or where it is discontinuous, the hydraulic conductivity is controlled by the liquid film component k_l^{Film}, although this is many orders of magnitude smaller than the hydraulic conductivity at high values of degree of saturation. Hence, k_l^{Bulk} is represented with a modified version of the Mualem (1976) model, which has k_l^{Bulk} going to zero when the bulk water becomes discontinuous, and k_l^{Film} is included through a semi-empirical expression.

The bulk water component k_l^{Bulk} (Scarfone et al., 2020) is calculated by using a modified version of the Mualem model (modM) which can be written as:

$$k_l^{Bulk} = k_{ls} \cdot \sqrt{S_l^C}\left[1-\left(1-\left(S_l^B\right)^{1/m}\right)^m\right]^2$$

(11)

where k_{ls} is the saturated hydraulic conductivity and m is the parameter of the modVG SWRC model. The terms S_l^C is defined by:

$$S_l^C = \frac{S_l - S_{l,BWD}}{S_{ls} - S_{l,BWD}} \quad \text{for drying}$$

(12a)

$$S_l^C = \frac{S_l - S_{l,BWC}}{S_{ls} - S_{l,BWC}} \quad \text{for wetting}$$

(12b)

where $S_{l,BWD}$ and $S_{l,BWC}$ are the values of degree of saturation at the bulk water-discontinuity (BWD) point and at the bulk water-continuity (BWC) point, namely when the bulk water becomes respectively discontinuous during drying and continuous during wetting. The terms S_l^B is defined by:

$$S_l^B = \frac{S_l - S_{l,BWEX}}{S_{ls} - S_{l,BWEX}} \quad \text{for drying}$$

(13a)

$$S_l^{\,B} = \frac{S_l - S_{l,BWE}}{S_{ls} - S_{l,BWE}} \quad \text{for wetting}$$

(13b)

where $S_{l,BWEX}$ and $S_{l,BWE}$ are the values of degree of saturation at the bulk water-exclusion point (BWEX) and at the bulk water-entry (BWE) point, namely when the bulk water is respectively expelled from the last pores during drying and enters the first pores during wetting. In the absence of more precise data, Scarfone et al. (2020) suggest to assume $S_{l,BWD}$=$S_{l,BWEX}$ and $S_{l,BWC}$=$S_{l,BWE}$ and that these two points are identified from experimental SWRC data with a simplified graphical procedure. According to this procedure, with the SWRC presented in the standard semi-logarithmic plot (S_l:log$s$), the intersection point of the tangent through the inflection point of the main drying curve and the straight line formed by the final linear portion of the main drying curve defines a suction $s_{BWD}/_{BWEX}$. The value of $S_{l,BWD}$=$S_{l,BWEX}$ is then taken as the value of S_l on the main drying curve at the suction $s_{BWD}/_{BWEX}$. A corresponding procedure using the main wetting curve gives the value of $S_{l,BWC}$=$S_{l,BWE}$.

The liquid film component of the hydraulic conductivity k_l^{Film} (Scarfone et al., 2020) is expressed by:

$$k_l^{Film} = C^{Film} \cdot \left(a^{Film} + s\right)^{-1.5}$$

(14)

a^{Film} is a dummy parameter only introduced to avoid k_l^{Film} tending to infinity when s tends to 0 but it must be small enough to have a negligible effect in the range of suction where the hydraulic conductivity is controlled by k_l^{Film} (i.e. when k_l^{Bulk} =0). C^{film} is a model parameter (soil constant) which can be calibrated experimentally if hydraulic conductivity data k_l:s are available at very low degree of saturation, i.e. in the range where the hydraulic conductivity is governed by the liquid film component k_l^{Film}. However, such data are rarely available and, in these cases, Scarfone et al. (2020) suggested that C^{Film} can be estimated as:

$$C^{Film} = X_D \frac{1-\phi}{D}$$

(15)

where ϕ is the porosity, D is a representative particle size and X_D is an empirical parameter (soil constant). In particular, Scarfone et al. (2020) suggested a value X_D=2.35x10^{-9} mm.ms^{-1}.kPa$^{1.5}$ for $D=D_{10}$ or a value X_D=1.08x10^{-8} mm.ms^{-1}.kPa$^{1.5}$ for $D=D_{50}$, regardless of the type of relatively coarse-grained soil (gravel, sand or silt).

It is now important to consider the implications of combining the new modM+LF SHCC model with the new hysteretic modVG SWRC model described earlier. The bulk water component of the SHCC k_l^{Bulk} is typically recognized as non-hysteretic when plotted against the degree of saturation (Fredlund and Rahardjo, 1993; Kool and Parker, 1987; Mualem, 1986; Vachaud and Thony, 1971), and thus hysteretic if plotted against suction, due to the hysteresis in the SWRC (see Figure 4). In order to satisfy the requirement that k_l^{Bulk} is non-hysteretic when plotted against S_l, the following restrictions must be applied to the parameters of the hysteretic modVG SWRC model and modM+LF SHCC model:

$$m_d\left(=1-1/n_d\right) = m_w\left(=1-1/n_w\right)$$

(16)

$$S_{l,BWC} = S_{l,BWD}$$

(17)

$$S_{l,BWE} = S_{l,BWEX}$$

(18)

All 3 of these restrictions are typically realistic (Likos and Godt, 2013). Under the assumptions of Equations 16, 17 and 18, Equation 11 gives a unique relationship between k_l^{Bulk} and S_l, irrespective of whether the soil state is on the main wetting curve, the main drying curve or a scanning curve (see Figure 4c).

The liquid film component of the hydraulic conductivity k_l^{Film} is still given by Equation 14, with a^{Film} and C^{Film} as soil constants, and thus k_l^{Film} is uniquely related to suction s, irrespective of whether the soil state is on the main drying curve, the main wetting curve or a scanning curve i.e. k_l^{Film} is non-hysteretic when plotted against s (see Figure 4b).

Figure 4 qualitatively shows the performance of the new hysteretic hydraulic modVG-modM+LF model in the S_l:s plot, the k_l:s plot and the k_l:S_l plot, by simulating a virtual sequence of wetting and drying paths (starting at point A and ending at point K). Results in Figure 4 were obtained assuming $S_{ls,d}$=$S_{ls,w}$=1, ξ_d=ξ_w and s_{dry}=1GPa. Under saturated conditions and at very low degree of saturation the water retention behaviour is non-hysteretic (see Figure 4a). Scanning curves (e.g. A-B) describe the hysteresis in the water retention behaviour at intermediate values of degree of saturation. The bulk water component of the hydraulic conductivity k_l^{Bulk} can be identified as the SHCC at medium and high values of degree of saturation (i.e. $S_l>S_{l,BWC/BWD}$ in Figure 4c) whereas the liquid film component k_l^{Film} can be identified as the hydraulic conductivity at very low degree of saturation (straight line in the k_l:s log-log plot in Figure 4b and $S_l<S_{l,BWC/BWD}$ in Figure 4c).

The bulk water component of the hydraulic conductivity k_l^{Bulk} is non-hysteretic when plotted against degree of saturation S_l (see Figure 4c) whereas k_l^{Bulk} is hysteretic when plotted against suction s (see Figure 4b) due to hysteresis in the SWRC. The liquid film component k_l^{Film} is non-hysteretic when plotted against suction s (see Figure 4b). From the physical point of view, the liquid film conductivity is related to the thickness of the liquid films, which is solely a function of suction for a given soil. At very low degree of saturation, k_l^{Film} is non-hysteretic also when plotted against S_l because only liquid film water and meniscus water are present and, in this condition, also the SWRC is non-hysteretic. However, k_l^{Film} is slightly hysteretic in the k_l:S_l plot at the transition between bulk water-dominated hydraulic conductivity and liquid film-dominated hydraulic conductivity (see Figure 4c), in particular for values of the degree of saturation between the BWC/BWD points and the BWE/BWEX points, i.e. $S_{l,BWE/BWEX}<S_l<S_{l,BWC/BWD}$. This prediction of the model has a physical explanation. Since $S_l<S_{l,BWC/BWD}$, bulk water is not continuous and the liquid flow is governed by the liquid film hydraulic conductivity but, since $S_l>S_{l,BWE/BWEX}$, a small amount of bulk water is present in the soil although it does not contribute to liquid flow. Hence, within this transition range, the bulk water influences the value of S_l but does not influence the value of k_l.

2.4 Experimental validation

Scarfone et al. (2020) showed that the modVG-modM+LF hydraulic model (without hysteresis) was able to match well experimental SWRC and SHCC data on main wetting or main drying curves over the full range of degree of saturation for a broad variety of relatively coarse-grained soils (gravels, sands and silts). In this current paper, the hysteretic aspects of the new hydraulic model for unsaturated soils are validated against experimental data for coarse-grained soils from the literature.

Figure 5 shows experimental SWRC data for Tottori sand (Rudiyanto et al., 2015), covering the full range of degree of saturation and including scanning drying and scanning wetting curves. Figure 5a shows results over the full range of suction (with suction on a logarithmic scale), whereas Figure 5b shows a zoom of the low suction range (with suction on a linear scale). The SWRCs are shown in terms of the volumetric water content

θ_l, which, assuming no deformation of the soil, can be expressed as $\theta_l=\theta_{ls}\cdot S_l$ where θ_{ls} is the water content when the soil is fully saturated.

The experimental SWRC data for Tottori sand were fitted using the hysteretic modVG model (see Figure 5). The primary drying curve and the main wetting curve were firstly best fitted to the corresponding experimental data. Note that the main wetting curve does not reach a fully saturated condition as suction approaches zero, indicating the likely occurrence of air trapping (i.e. this was an apparent SWRC, rather than a true SWRC). Hence, a value of S_{ls} less than 1 was selected to fit the main wetting curve. Subsequently, the scanning curves were fitted by imposing the curves to pass through the previous reversal point and fitting Equation 6a or 6b to the experimental data, where γ_d for drying and γ_w for wetting were the only fitting parameters. Table 1 shows the model parameters obtained with this procedure. Note that $\xi_d=\xi_w$ but $n_d>n_w$ and $\gamma_d>\gamma_w$. The hysteretic modVG model fits well the experimental SWRC data for the main drying curve and main wetting curve over the full range of degree of saturation, and it also fits well the single scanning drying curve and the single scanning wetting curve.

Scarfone (2020) showed that the experimental SWRC data for Tottori sand shown in Figure 5 could also be successfully fitted by the hysteretic modBC and hysteretic modK SWRC models mentioned earlier, although the fit achieved by the hysteretic modBC model was slightly less satisfactory than the other two models.

Figure 6 shows the comparison between the hysteretic modVG model and experimental SWRC data for Wray sand obtained by Gillham et al. (1976). For this soil, different scanning drying curves (see Figure 6b) and different scanning wetting curves (see Figure 6c) were available. The modVG model was initially best fitted to the experimental main drying and main wetting curves (see Figure 6a). Subsequently, all the experimental scanning curves of a family, i.e. wetting or drying, were fitted by the hysteretic modVG model using a single value for γ_d (for all scanning drying curves) or γ_w (for all scanning wetting curves). The parameter values are shown in Table 1. Note that $S_{ls,d}$=$S_{ls,w}$=1 and the values of ξ_d and ξ_w are very similar, but n_d>n_w and γ_d>γ_w. From Figures 6b and 6c, it can be seen that the model provided a very good fit to all the scanning curves. Therefore, the use of a single pair of values for the parameters γ_d and γ_w was sufficient to model the different scanning curves starting from different reversal points.

Figure 7 shows experimental data for aggregated glass beads from Topp and Miller (1966), covering SWRC curves and SHCC curves (k_l:θ_l) for primary drying, main wetting and main drying (Figures 7a and 7b), together with a family of 5 scanning drying SWRC curves (Figure 7c) and a family of 6 scanning wetting SWRC curves (Figure 7d). Primary drying, main drying and main wetting SWRC experimental data were fitted by the modVG model assuming a single value of ξ for all three curves, but allowing different values of n for the three curves. The scanning SWRCs were fitted by the hysteretic modVG model using a single value of γ_d or γ_w for each family of scanning curves, as described for the Wray sand. The primary drying, main drying and main wetting SHCCs were predicted using the modM+LF model, assuming the constraints given by Equations 17 and 18 (the constraint of Equation 16 was not imposed, as a consequence of the decision to allow different values of n for the three SWRCs). The resulting model parameters are shown in Table 2. Note that S_{ls}<1 for the main wetting curve and the main drying curve, indicating the likely occurrence of air trapping during wetting (see Figure 7a).

The experimental primary drying, main wetting and main drying SWRCs for aggregated glass beads were fitted satisfactorily by the modVG model (see Figure 7a). As was observed for the Wray sand (see Figure 6), the use of a single value for γ_d and a single value for γ_w for the aggregated glass beads led to very good fitting of the scanning drying SWRC curves (see Figure 7c) and the scanning wetting SWRC curves (see Figure 7d).

Inspection of the experimental and predicted SHCCs for the aggregated glass beads (see Figure 7b), presented as the ratio of hydraulic conductivity to saturated hydraulic conductivity k_l/k_{ls} plotted against volumetric water content θ_l, shows that the experimental measurements of k_l did not extend into the range where the hydraulic conductivity was controlled by flow in liquid films. According to the model predictions, $k=k^{Film}$ for $S_l<S_{l,BWC/BWD}$, corresponding to $\theta_l<0.09$, and the predicted values of k_l/k_{ls} are then less than 10^{-6} (see Figure 7b and compare with Figure 4c). Experimental validation of modVG-modM+LF predictions of hydraulic conductivity in this domain controlled by flow in liquid films was presented for a range of other soils by Scarfone et al. (2020), but for experimental data from the literature that did not include both drying and wetting paths (i.e. there was no opportunity to examine the presence or absence of hysteresis).

The experimental values of k_l/k_{ls} shown in Figure 7b confirm very little hysteresis when plotted against θ_l (or S_l), as expected for the range where hydraulic conductivity is controlled by bulk water flow. Very careful inspection of the experimental data suggests a very small amount of hysteresis, with values of k_l/k_{ls} being slightly greater on the primary drying curve and slightly smaller on the main wetting curve than they are on the main drying curve. Interestingly, this very small amount of hysteresis is also captured in the model predictions, because of the use of different values of n for the three curves (i.e. because the constraint of Equation 16 was not imposed).

Comparison of the model predictions and the experimental measurements in Figure 7b shows that the modVG-modM+LF model provides a good match to the experimental data for θ_l>0.18 and correctly captures the fact that k_l/k_{ls} tends to extremely low values as θ_l approaches 0.09 (corresponding to k^{Bulk} tending to zero at $S_{l,BWC/BWD}$). However, the fit of the model predictions is less good in the range immediately above $S_{l,BWC/BWD}$, suggesting a minor weakness of the modVG-modM+LF model when applied to this highly idealised soil (or problems with the experimental measurements at these relatively low values of θ_l, when much longer time durations are required to ensure proper equalisation of suction throughout a soil sample, because of the much lower values of k_l). It is important to emphasise that the experimental data shown in Figure 7b were not used at all in determining the model parameter values.

3. Application of the hysteretic hydraulic constitutive model in a numerical study of capillary barrier systems

The new hysteretic modVG-modM+LF hydraulic constitutive model was implemented in the Code_Bright finite element software (Olivella et al., 1996). This code was then used to perform one-dimensional numerical simulations of infiltration and evaporation processes in a capillary barrier system (CBS). Initial simulations, presented by Scarfone et al. (2020), did not include the hysteretic aspects of the hydraulic constitutive model. These initial simulations demonstrated that the improvements at low values of degree of saturation contained within the modVG-modM+LF hydraulic constitutive model are essential for correct simulation of the phenomenon of breakthrough in a CBS. The purpose of the subsequent numerical simulations presented in this paper was to assess the role of hydraulic hysteresis in the fundamental hydraulic behaviour of CBSs. Surprisingly, water retention hysteresis has often been neglected in numerical modelling of the hydraulic behaviour of CBSs but, as will be shown in this section, it may have a significant role.

Retention hysteresis will affect the behaviour of a CBS if individual soil elements within the CBS experience reversals of wetting and drying. Hence, the numerical study reported here examined the influence of retention hysteresis under 3 different situations: i) redistribution of water within the finer layer if rainfall ceases prior to any breakthrough of water to the coarser layer; ii) conditions at breakthrough (if sustained rainfall occurs) and on subsequent restoration of the CBS if rainfall then ceases after breakthrough; and iii) during alternating periods of rainfall and evaporation from the ground surface. Restoration of the CBS (after breakthrough has occurred) is the condition where water stops flowing across the interface between finer and coarser layers, some time after water infiltration at the ground surface ceases (Stormont and Anderson, 1999).

3.1 Numerical models

The numerical model consisted of a vertical column of soil made of two layers: an upper layer, 0.5m thick, representing the finer layer (F.L.) of a CBS and a lower layer, 0.75m thick, representing the coarser layer (C.L.) (see Figure 8a). The thickness of the coarser layer was unrealistically high in order to have the bottom boundary sufficiently far from the interface that the phenomenon of breakthrough at the interface between F.L. and C.L. was not affected by any influence of the bottom boundary.

In all analyses, the solid phase was considered as non-deformable and the gas phase as non-mobile, with a constant and uniform value of pore-gas pressure p_g=100kPa (pore-gas pressure p_g and pore-liquid pressure p_l were both expressed as absolute pressures). The simulations involving the study of the effects of water retention hysteresis on i) water redistribution within the finer layer and ii) breakthrough and restoration conditions were isothermal and a constant and uniform distribution of temperature was imposed, with T=20°C. The simulations involving the study of the effects of water retention hysteresis on iii) evaporation from the ground surface were non-isothermal (i.e. thermo-hydraulic), with heat conduction modelled by Fourier's Law, and vapour diffusion in the gas phase (modelled by Fick's Law) was also included. Heat convection, i.e. the heat flux associated to the mass fluxes of water and air, calculated as the product of the mass flux and the corresponding internal energy, was also included in the thermo-hydraulic analyses.

The materials forming the two layers were each modelled by defining the hydraulic constitutive models (SWRC and SHCC), together with the values of saturated hydraulic conductivity k_{ls} and porosity ϕ. In addition, in the thermo-hydraulic simulations, the parameters modelling the thermal conductivity and the vapour diffusivity were also defined. Each of the two layers was considered as a uniform material. The parameters chosen to model the finer layer were representative of a fine sand (Scarfone, 2020) whereas those of the coarser layer were representative of a gravelly sand (Tami et al., 2004). The hydraulic behaviour of the materials was modelled using the modVG-modM+LF model. In the simulations, the hydraulic behaviour of both the finer layer and the coarser layer was modelled using three different SWRC models: a unique curve corresponding to the main wetting curve (W), a unique curve corresponding to the main drying curve (D) and the full hysteretic model (H) (i.e. including the main wetting curve, the main drying curve and the scanning curves). The comparison of the results obtained using these three models highlights the role of water retention hysteresis in the modelling of the fundamental behaviour of CBSs. The parameter values of the materials are shown in Table 3 and the SWRCs and SHCCs are shown in Figures 8c and 8d respectively.

The numerical simulations that were performed were divided into three different stages (1a, 1b and 2). Stage 1a analysed the effect of hydraulic hysteresis on water redistribution occurring in the finer layer if rainfall ceased after a short period of intense rain that was insufficient to cause water breakthrough to the coarser layer. Stage 1b analysed the effect of hydraulic hysteresis on the behaviour of a CBS at breakthrough and at subsequent restoration. Stage 2 studied the effect of hydraulic hysteresis during alternating periods of rainfall and evaporation from a CBS to the atmosphere.

In stage 1a, the initial pore-liquid pressure profile (see Figure 8b) consisted of a hydrostatic distribution in the C.L., varying between p_l=100kPa (s=0kPa) at the bottom and p_l=92.5kPa (s=7.5kPa) at the interface, and a constant value of p_l in the F.L., p_l=75kPa (s=25kPa). As a consequence, as shown by the initial degree of saturation profile shown in Figure 8b, the F.L. and C.L. were initially almost dry, excluding the bottom few centimetres of the C.L. (which did not affect any of the results shown in this paper), and hence main wetting and drying curves are indistinguishable in this range of degree of saturation values. The discontinuity of the suction profile initially present at the interface between the finer layer and the coarser layer had negligible impact on the results. In stage 1a, a liquid water flow rate varying with time was imposed at the top boundary (soil surface). As shown in Figure 9a, a high infiltration rate (a mass flow rate per unit plan area P of 2×10^{-1}kg/(m^{2}s), corresponding to a volumetric infiltration rate per unit plan area i of approximately 2×10^{-4}m/s) was imposed at the top boundary for 5 minutes. The infiltration at the ground surface was then stopped and replaced by an impermeable boundary condition (i.e. P=0 kgs^{-1}m^{-2}) at the top boundary. In this subsequent period, redistribution of water occurred within the finer layer, and this redistribution had almost finished after 10 days. After 10 days, the cycle of boundary condition at the top boundary was repeated, i.e. another 5 minutes of intense infiltration rate and then no infiltration until

20 days. In stage 1a, the total amount of water entering at the top boundary was insufficient to cause water breakthrough across the interface. A fixed value of pore-liquid pressure p_l=100kPa (s=0kPa) was imposed at the bottom boundary.

In stage 1b, the simulations continued from the end of stage 1a (t=20days). The bottom boundary condition in stage 1b still consisted of a fixed pore-liquid pressure p_l=100kPa (s=0kPa). At the top boundary (see Figure 9b), a relatively slow infiltration rate was applied (P=10^{-4}kgs^{-1}m^{-2}, corresponding approximately to i=10^{-7}m/s) for 20 days (from t=20days to t=40days). During this time, breakthrough occurred with all the models (W, D and H). At t=40 days, the infiltration was ceased and the simulation was run for another 20 days (from t=40days to t=60days), with an impermeable boundary condition at the ground surface. Restoration of the CBS (cessation of water flow across the interface between F.L. and C.L.) occurred during this final period.

In stage 2, non-isothermal simulations were performed in which water vapour diffusion within the gas phase in the soil pores was also included. Initial hydraulic conditions were the same as imposed in stage 1a (see Figure 8b). In addition, an initial uniform temperature profile, with T=25°C was prescribed. A fixed pore-liquid pressure p_l=100kPa (s=0kPa) was again imposed at the bottom boundary. At the top boundary, an "atmospheric" boundary condition was applied. This included rain P and evaporation E for the mass transfer, and radiation R_n, sensible heat flux (advection) H_s and latent heat flux H_c (convection) for the energy transfer. The evaporation E was modelled as (Brutsaert, 1982):

$$E = \frac{k^2 v_a \psi}{\ln\left(z_a / z_0\right)^2}\left(\rho_v - \rho_{va}\right)$$

(19)

where k is Von Karman's constant (k=0.4), z_a is the screen height, v_a is the wind speed at the screen height, ψ is the stability factor, z_0 is the roughness length, ρ_{va} is the absolute humidity of the atmosphere at the screen height and ρ_v is the absolute humidity in the gas phase within the soil pores at the soil surface (i.e. boundary nodes). ρ_{va} is a is a function of atmospheric air temperature T_a, atmospheric relative humidity RH_a and atmospheric gas pressure p_{ga}, whereas ρ_v is a function of soil surface temperature T, pore-liquid pressure p_l and pore-gas pressure p_g. These relationships are governed by the psychrometric law. Thermo-hydraulic analyses were required within the soil, in order to calculate the soil surface temperature T, which affected the corresponding absolute humidity within the soil pores ρ_v and hence the evaporation E from the soil surface through Equation 19. The sensible heat flux H_s was modelled as (Brutsaert, 1982):

$$H_s = \frac{k^2 v_a \psi}{\ln\left(z_a / z_0\right)^2} \rho_{ga} C_a \left(T - T_a\right)$$

(20)

where ρ_{ga} is the atmospheric gas density, C_a is the specific heat of the gas, T_a is the atmospheric temperature at the screen height and T is the soil surface temperature.

In stage 2, the atmospheric boundary condition imposed at the soil surface (top boundary), consisted of multiple cycles of rain and evaporation, as shown in Figure 9c. Each cycle, lasting 12 hours, was composed of 30 minutes of intense rainfall (P=10^{-2}kgs^{-1}m^{-2}, corresponding approximately to i=10^{-5}m/s) and 11 hours and 30 minutes of evaporation. Evaporation was not active during rainfall. The evaporation and the different boundary heat fluxes were the result of the assigned atmospheric parameters shown in Table 4. These atmospheric parameter values are representative of a soil surface covered by short grass and of summer weather conditions in Cagliari (Italy) (Servizio

Metereologico Aeronautica Militare, 2018). 20 cycles of rain and evaporation were simulated, for a total duration of 240 hours.

3.2 Results and discussion

3.2.1 Stage 1a: water redistribution prior to breakthrough

Numerical simulations of stage 1a were performed to analyse the role of water retention hysteresis during water redistribution within the finer layer after intense rainfall events (see Figure 9a). Figure 10 shows suction and degree of saturation profiles obtained at different times in stage 1a, using the main wetting curve model (W), the main drying curve model (D) and the full hysteretic model (H). The results at 4 key times are shown: *t*=5minutes, *t*=10days, *t*=10days and 5minutes and *t*=20days which are respectively the end of the first intense rainfall event (Figures 10a,e), the end of the water redistribution period following the first intense rainfall event (Figures 10b,f), the end of the second intense rainfall event (Figures 10c,g) and the end of the water redistribution period following the second intense rainfall event (Figures 10d,h).

At the end of the first intense rainfall event (*t*=5minutes) (see Figures 10a,e), a sharp wetting front is located at a height of approximately 1.1m. Above this wetting front, the soil of the finer layer is almost saturated whereas, below the wetting front, the CBS is approximately in the initial condition. This type of infiltration pattern is typical of high ratios of infiltration rate i compared to unsaturated hydraulic conductivity k_l (Zhang et al. 2004, Zhan and Ng, 2004), i.e. high values of i/k_l. At this time (*t*=5minutes), the results obtained with the H model coincide with the results obtained with the W model because the soil above the wetting front has experienced only wetting and the remainder of the soil in the CBS has not experienced any significant wetting or drying. Slightly higher suction values are predicted with the D model close to the soil surface.

After the first intense infiltration event, water redistribution occurs within the finer layer, with water draining down from the upper part of the F.L. to the lower part of the F.L. This water redistribution has almost ceased after 10 days. At t=10 days, different suction profiles and degree of saturation profiles are predicted with the different models (see Figures 10b,f). The suction profile in the finer layer obtained with the H model is intermediate between the profiles obtained with the W model and the D model (see Figure 10b). However, a different pattern is found in the degree of saturation profiles in the finer layer (see Figure 10f). In contrast with the profiles obtained with the W model and the D model, which show S_l monotonically increasing through the F.L. from the ground surface to the interface with the C.L., the degree of saturation profile obtained with the H model shows S_l increasing from the ground surface (point E) to point D, decreasing from point D to point B and finally increasing from point B to the interface (point A).

The degree of saturation profiles obtained in the finer layer after 10 days with the H model (Figure 10f) can be interpreted more clearly if plotted in the s:S_l plane and compared with the adopted SWRCs of the finer layer, as shown in Figure 11a. From Figure 11a, it can be seen that, after 10 days, the hydraulic states of the soil at heights between point A and point B lie almost on the main wetting curve, between point D and point E they lie almost on the main drying curve and between point B and D they lie on different scanning curves. The following interpretation can be given. During the initial intense rainfall event, the soil in the upper part of the finer layer (from point D to point E) reaches high values of degree of saturation and low values of suction. When infiltration is stopped, the water in this zone starts flowing downwards and the soil in the upper part of the finer layer dries significantly. Hence, the soil between points D and E moves along scanning drying curves and almost onto the main drying curve (see the scanning drying curve followed by the soil at point D, indicated by a dashed line in Figure 11a). A similar process occurs in the soil at heights between points B and D but, in this case, the first wetting does not cause such high values of degree of saturation and the subsequent increase of suction due to drying is not sufficient to bring the soil state close to the main drying curve (see the scanning drying curve followed by the soil at point C, indicated by a second dashed line in Figure 11a). Therefore, the hydraulic states of the soil at heights between point B and point D are located on different scanning curves. Finally, the soil at heights between point A and point B experience only main wetting paths because these points experience only monotonic wetting.

At the end of the second rainfall event (t=10days and 5minutes) (see Figures 10c,g), the soil in the upper part of the finer layer is almost saturated and, below a sharp wetting front, the suction and degree of saturation profiles are approximately coincident with those obtained before the beginning of the second rainfall event.

At the end of the second water redistribution period (t=20days) (see Figures 10d,h), the patterns obtained in the suction and degree of saturation profiles are similar to those obtained at t=10days. The graphical interpretation in the s:S_l plot of the hydraulic states of the soil in the finer layer is shown in Figure 11b. In this case, the higher amount of water stored in the finer layer leads to higher values of degree of saturation and lower values of suction, but the phenomenon of water redistribution within the finer layer of the CBS can be interpreted in the same way as at t=10days.

Generally speaking, the modelling of water retention hysteresis leads to significantly different predictions of the redistribution of water in the finer layer of a CBS after intense rainfall events than is predicted by using a unique SWRC (irrespective of whether this is a main wetting curve or a main drying curve). Given that rainfall events produce mainly wetting in the soil, it might be expected that the main wetting curve alone would be adequate to model the situation of stage 1a. However, the redistribution of water generates wetting in the lower part of the finer layer and drying in the upper part of the finer layer. This explains why the use of the hysteretic model leads to different results compared to the use of only the main wetting curve. Moreover, in contrast with what might be expected, the degree of saturation profiles obtained with the H model are not intermediate between the profiles obtained with the W model and the D model. In particular, the use of the H model leads to the prediction of more similar values of S_l at the top and bottom of the finer layer than is predicted by the W or D models (see Figures 10f and 10h).

3.2.2 Stage 1b: breakthrough and restoration

Numerical simulations of stage 1b were performed to analyse the role of water retention hysteresis in water breakthrough from the finer layer to the coarser layer of a CBS and the subsequent restoration of the barrier after breakthrough if rainfall ceases. The study of the conditions at breakthrough is of primary importance for understanding the water storage capacity of a CBS (Stormont and Morris, 1998; Stormont and Anderson, 1999), i.e. the maximum amount of water that can be stored in the finer layer before breakthrough occurs. The study of the conditions at restoration is of primary importance for understanding the ability of a CBS to partially recover its water storage capacity after breakthrough has occurred and then rainfall ceases (Stormont and Anderson, 1999).

Figure 12a shows the time histories of the downward liquid flows occurring across the interface between finer layer and coarser layer, predicted with the W model, the D model and the H model, following the onset and cessation of a sustained period of rain (from

t=20 days to t=40 days). Figure 12b shows the corresponding time histories of suction at the interface. The times at breakthrough, identified as the time at which water flow across the interface first dramatically increases, and at restoration, identified as the time at which water flow across the interface almost stops (some time after water infiltration at the ground surface ceases), are marked by symbols in Figures 12a and 12b. It should be noted that significantly different times at breakthrough are predicted with the different models: the earliest is obtained with the W model and the latest with the D model. Accordingly, the highest water storage capacity is predicted with the D model and the lowest with the W model. Restoration of the CBS occurs very soon after rainfall ceases (at t=40 days) in all 3 cases (see Figure 12a).

Before breakthrough, as infiltration at the ground surface occurs, the suction at the interface between F.L. and C.L. predicted by all three models decreases (see Figure 12b), because of the wetting of the finer layer. Suction at the interface then stops decreasing when water breakthrough across the interface commences. According to the W and H models, breakthrough starts approximately when suction at the interface attains the bulk water-continuity value of suction s_{BWC} of the coarser layer, whereas according to the D model, breakthrough starts approximately when suction at the interface attains the bulk water-discontinuity value of suction s_{BWD} (see Figure 12b). These soil states at the time of breakthrough are indicated in Figure 13, with their relationships to the main drying curve and the main wetting curve of the coarser layer.

According to the W model and the D model, the suction at the interface after breakthrough remains almost constant at the breakthrough value until infiltration at the ground surface ceases (at t=40 days), soon after which restoration occurs and the suction at the interfaces then slowly increases (see Figure 12b). In contrast, according to the H model, the suction at the interface shows a small step increase from the breakthrough value s_{BWC} immediately after breakthrough occurs and it then remains constant until water infiltration at the ground surface ceases, at which point it shows another step increase to s_{BWD}, when restoration occurs (see Figure 12b). This behaviour is indicated in Figure 13, which shows breakthrough and restoration states at the top of the coarser layer predicted by the 3 models. Post-restoration, the H model predicts that the gradual increase of suction at the interface occurs more quickly than is predicted by the W and D models (see Figure 12b). The small step increase of suction (approximately 0.15kPa) predicted after breakthrough with the H model can be physically explained as follows. When breakthrough occurs, a small amount of bulk water suddenly moves from the finer layer to the smaller voids of the coarser layer close to the interface. This water movement causes a very small (undetectable) decrease of water content in the finer layer (i.e. following a drying path), which corresponds to a small but noticeable increase of suction, due to the shallow gradient of the drying scanning curve starting from the BWC point.

Of the results presented in Figure 12b, only the predictions of the H model qualitatively agree with the behaviour of CBSs observed experimentally by Stormont and Anderson (1999). They showed that, at breakthrough, the suction at the interface attains the BWC value of the coarser layer, identified as the bend in the main wetting SWRC at low degree of saturation. They also observed that, after infiltration at the ground surface ceases and water breakthrough stops, this suction at the interface significantly increases due to the effect of water retention hysteresis, thereby leading to restoration of the capillary barrier effect. Therefore, whereas the W model may be adequate to represent the hydraulic behaviour of the CBS up to breakthrough it is not able to represent correctly the restoration conditions. On the other hand, the D model is able to capture the restoration conditions but it is unable to correctly represent the hydraulic behaviour of the CBS at breakthrough. Only the hysteretic model is able to represent adequately both the breakthrough conditions and the restoration of the CBS after breakthrough.

3.2.3 Stage 2: effect of evaporation

Stage 2 was simulated to study the effect of hydraulic hysteresis on the prediction of evaporation to the atmosphere from a CBS. The CBS, which was initially almost dry, was subjected to 20 cycles of 30 minutes of rain and 11 hours and 30 minutes of evaporation (see Figure 9c), corresponding to relatively hot and dry weather conditions (i.e. representative of summer conditions in Cagliari, Italy).

Figure 14 shows the results of the simulations, in the form of time histories of (a) evaporation rate, (b) cumulative evaporation, (c) water flow rate across the interface and (d) cumulative inflow and outflow into/from the finer layer. The cumulative evaporation in Figure 14b was obtained by integrating the evaporation rate over time. In Figure 14d, the cumulative inflow to the finer layer at the ground surface was obtained by integrating over time the rain minus evaporation, the cumulative outflow from the finer layer to the coarser layer was obtained by integrating over time the water flow rate across the interface and finally the cumulative net inflow to the finer layer was calculated as the difference between the cumulative inflow at the ground surface and the cumulative outflow to the coarser layer.

In the first 7 cycles (0h<t<84h), the evaporation fluxes predicted with the W and D models almost coincide whereas the evaporation predicted with the H model is, in cumulative terms, significantly higher (see Figures 14a and 14b). In each cycle, the evaporation predicted with the W and D models is initially high but it rapidly decreases, whereas the evaporation predicted with the H model remains relatively high during the full duration of each evaporation period (see Figure 14a). These different evaporation patterns can be better understood by inspection of the corresponding degree of saturation profiles at the beginning of a cycle (e.g. t=72.5h) and at the end of the same cycle (e.g. t=84h), as shown in Figures 15a and 15b. At the beginning of a cycle, when the evaporation rate predicted by all the models is relatively high (see Figure 14a), the degree of saturation values at the soil surface predicted with all the models are relatively high (see Figure 15a). By contrast, at the end of a cycle, when the evaporation rate predicted with the H model is still relatively high but that predicted with the W and D models is much lower (see Figure 14a), the degree of saturation at the surface predicted with the H model is moderately high whereas that predicted with the W and D models is very low, approaching zero (see Figure 15b). This is in agreement with the fact that the evaporation from wetter soil surfaces occurs at a higher rate (Brutsaert, 1982). In other words, with the H model the water distribution is predicted to be more uniform in the finer layer compared to the W and D models. With the H model, the higher availability of water close to the surface allows higher evaporation rates to be sustained for longer times.

For subsequent cycles (in particular for t>120h), the evaporation rate predicted with the W model follows the same patterns as before whereas the evaporation rate predicted with the D model coincides with that predicted with the H model (see Figures 14a and 14b). This can again be better understood by observing the degree of saturation profiles at the beginning of a cycle (e.g. t=228.5h) (see Figure 15c) and at the end of the same cycle (e.g. t=240h) (see Figure 15d). At the beginning of the cycle, relatively high values of degree of saturation at the surface were predicted with all the models (see Figure 15c) as well as relatively high evaporation rates (see Figure 14a). In these later cycles, the amount of water stored in the F.L. is greater than during the initial cycles (compare Figures 15c and 15a) and the water stored close to the surface predicted with the D model is now much higher, even higher than that predicted with the H model. Consequently, at the end of the cycle (see Figure 15d), the degree of saturation values predicted with the D and H models at the surface both remain relatively high whereas the degree of saturation value predicted with the W model at the surface is very low, approaching zero.

The outflow from the finer layer through the interface (i.e. water breakthrough from the finer layer to the coarser layer) (see Figure 14c and the dashed lines in Figure 14d) is a result of the effects of the evaporation and of the water storage capacity of the CBS. Breakthrough is predicted to start after a lower number of cycles with the W model and, in each cycle, a higher total volume of water flows from the finer layer to the coarser layer. This is due to the low cumulative evaporation and low water storage capacity of the CBS when the W model is used. Comparing the predictions of the H model and of the D model, water breakthrough predicted with the H model starts one cycle earlier than water breakthrough predicted with the D model because a slightly lower water storage capacity of the CBS is predicted with the H model. After breakthrough has started, similar increases of cumulative water outflow during each cycle are predicted by the H and D models, because the cumulative evaporations are similar with both models.

In general, compared to the use of the main wetting curve alone or the main drying curve alone, the use of the full hysteretic model leads to significantly different predictions of the thermo-hydraulic response of the CBS when subjected to cycles of rain and evaporation. Therefore, the lack of consideration of hydraulic hysteresis in the simulation of the cyclic behaviour of CBSs may lead to unreliable results. Higher evaporation rates are in general predicted using the H model, as also confirmed by the results of Zhang et al. (2009). The water storage capacity of the finer layer and the amount of percolation into the coarser layer predicted with the H model are intermediate between those predicted with the W model and those predicted with the D model.

4. Conclusions

In this paper, a new hysteretic hydraulic constitutive model for unsaturated soils improved at low degree of saturation is presented and validated against experimental soil water retention curve (SWRC) and soil hydraulic conductivity curve (SHCC) data. After implementation in the Code_Bright FE software, the new hysteretic hydraulic constitutive model has been applied to the numerical study of the hydraulic behaviour of capillary barrier systems (CBSs).

In the new hysteretic hydraulic constitutive model, main wetting and main drying SWRCs are modelled using a modified version of the van Genuchten model, improved at low degree of saturation. Scanning curves are modelled using a bounding surface approach, which leads to simple closed-form expressions for the scanning curves.

The SHCC model is improved at low degree of saturation, by distinguishing between the contributions to the hydraulic conductivity of liquid flow within bulk water and liquid flow within water films covering the surfaces of soil particles. Introducing certain parameter constraints in the hysteretic SWRC model means that the bulk water component of hydraulic conductivity k_l^{Bulk} is assumed non-hysteretic when plotted against degree of saturation S_l, whereas the liquid film component k_l^{Film} is non-hysteretic when plotted against suction s.

The new hysteretic hydraulic constitutive model has been validated against experimental SWRC and SHCC data from different soils. The model is able to represent well the hysteretic hydraulic behaviour of relatively coarse-grained unsaturated soils (gravels, sands and silts) over the full range of degree of saturation. Moreover, the model is easy to apply (it involves simple closed-form expressions), it is flexible (the same approach can be applied with other expressions for the main drying and main wetting SWRCs) and it requires a relatively low number of parameters (once the main SWRCs are defined, only a single pair of additional parameters, γ_d and γ_w, are required for the definition of the scanning SWRC curves and only two more parameters, the saturated hydraulic conductivity k_{ls} and C^{Film}, are required to define the SHCC behaviour). In addition, the simplicity of the model makes it suitable for implementation in numerical codes, as was done for Code_Bright.

After implementation in Code_Bright, the new hysteretic hydraulic constitutive model was applied in a numerical study of the effect of hydraulic hysteresis on the behaviour of CBSs. It is shown that inclusion of water retention hysteresis leads to significantly different predictions of the redistribution of water in the finer layer of a CBS after intense rainfall events, compared to predictions employing a unique SWRC. The full hysteretic constitutive model leads to a more uniform distribution of water in the finer layer after redistribution. The reason why use of a unique SWRC based on the main wetting curve is not adequate, even when there is no evaporation or other removal of water from a CBS, is that redistribution of water within the finer layer after rainfall ceases means that the upper part of the finer layer experiences drying during this redistribution.

The numerical study of CBSs also demonstrated that only the full hysteretic constitutive model is able to represent successfully both the condition at breakthrough (with suction at the interface attaining the BWC point of the coarser layer) and the condition at restoration of the CBS (with suction at the interface attaining the BWD point of the coarser layer). Finally, it is shown that hydraulic hysteresis has a major impact on the prediction of evaporation from a CBS to the atmosphere, because the hysteresis leads to higher water availability in the soil close to the ground surface and hence to the prediction of higher cumulative evaporation.

Acknowledgements

The authors wish to acknowledge the support of the European Commission via the Marie Skłodowska-Curie Innovative Training Networks (ITN-ETN) project TERRE 'Training Engineers and Researchers to Rethink geotechnical Engineering for a low carbon future' (H2020-MSCA-ITN-2015-675762).

References

Brooks R, Corey T. Hydraulic properties of porous media. *Hydrology Papers, Colorado State University*. 1964; 3:1–27.

Brutsaert W. *Evaporation into the atmosphere: Theory, History and Applications*. 299 pp., D. Reidel, Dordrecht; 1982.

Campbell G, Shiozawa S. Prediction of hydraulic properties of soils using particle-size distribution and bulk density data. *Indirect methods for estimating the hydraulic properties of unsaturated soils*. 1992; 317–328.

Dane JH, Wierenga PJ. Effect of hysteresis on the prediction of infiltration, redistribution and drainage of water in a layered soil. *Journal of Hydrology*. 1975; 25(3-4):229–242.

Fayer MJ. *UNSAT-H version 3.0: Unsaturated soil water and heat flow model theory, user manual, and examples*. Pacific Northwest National Lab., Richland, WA (US); 2000.

Fayer MJ, Simmons CS. Modified soil water retention functions for all matric suctions. *Water Resources Research*. 1995; 31(5):1233–1238.

Fredlund DG, Rahardjo H. *Soil mechanics for unsaturated soils*. John Wiley & Sons; 1993.

Gallipoli D, Bruno AW, D'Onza F, Mancuso C. A bounding surface hysteretic water retention model for deformable soils. *Géotechnique*. 2015; 65(10):793-804.

Gallipoli D, Wheeler SJ, Karstunen M. Modelling the variation of degree of saturation in a deformable unsaturated soil. *Géotechnique*. 2003; 53(1):105-112.

Gillham R, Klute A, Heermann D. Hydraulic properties of a porous medium: Measurement and empirical representation 1. *Soil Science Society of America Journal*. 1976; 40(2):203–207.

Haines WB. Studies in the physical properties of soil. V. The hysteresis effect in capillary properties, and the modes of moisture distribution associated therewith. *The Journal of Agricultural Science*. 1930; 20(1): 97-116.

Hanks RJ, Klute A, Bresler E. A numeric method for estimating infiltration, redistribution, drainage, and evaporation of water from soil. *Water Resources Research*. 1969; 5(5):1064–1069.

Jaynes D. Comparison of soil-water hysteresis models. *Journal of Hydrology*. 1984; 75(1-4):287–299.

Khalili N, Habte M, Zargarbashi S. A fully coupled flow deformation model for cyclic analysis of unsaturated soils including hydraulic and mechanical hystereses. *Computers and Geotechnics*. 2008; 35(6):872–889.

Khire MV, Benson CH, Bosscher PJ. Capillary barriers: Design variables and water balance. *Journal of Geotechnical and Geoenvironmental Engineering*. 2000; 126(8):695–708.

Khlosi M., Cornelis WM, Gabriels D, Sin G. Simple modification to describe the soil water retention curve between saturation and oven dryness. *Water Resources Research*. 2006; 42(11).

Klausner Y. *Fundamentals of continuum mechanics of soils*. Springer Science & Business Media; 2012.

Klute A, Heermann D. Soil water profile development under a periodic boundary condition. *Soil Science*. 1974; 117(5):265–271.

Kool J, Parker JC. Development and evaluation of closed-form expressions for hysteretic soil hydraulic properties. *Water Resources Research*. 1987; 23(1):105–114.

Kosugi KI. Lognormal distribution model for unsaturated soil hydraulic properties. *Water Resources Research*. 1996; 32(9):2697-2703.

Li X. Modelling of hysteresis response for arbitrary wetting/drying paths. *Computers and Geotechnics*. 2005; 32(2):133–137.

Likos WJ, Lu N, Godt JW. Hysteresis and uncertainty in soil water-retention curve parameters. *Journal of Geotechnical and Geoenvironmental Engineering*. 2013; 140(4):04013050.

Mualem Y. A new model for predicting the hydraulic conductivity of unsaturated porous media. *Water resources research*. 1976; 12(3):513-522.

Mualem, Y. Hydraulic conductivity of unsaturated soils: prediction and formulas. *Methods of Soil Analysis: Part 1 Physical and Mineralogical Methods*. 1986; 5:799–823.

Nuth M, Laloui L. Advances in modelling hysteretic water retention curve in deformable soils. *Computers and Geotechnics*. 2008; 35(6):835–844.

Olivella S, Gens A, Carrera J, Alonso E. Numerical formulation for a simulator (code_bright) for the coupled analysis of saline media. *Engineering computations*. 1996; 13(7):87–112.

Parker J, Lenhard R. A model for hysteretic constitutive relations governing multiphase flow: 1. saturation-pressure relations. *Water Resources Research*. 1987; 23(12):2187–2196.

Pedroso DM, Sheng D, Zhao J. The concept of reference curves for constitutive modelling in soil mechanics. *Computers and Geotechnics*. 2009; 36(1-2):149–165.

Peters, A. Simple consistent models for water retention and hydraulic conductivity in the complete moisture range. *Water Resources Research*. 2013; 49(10), 6765-6780.

Pham HQ, Fredlund DG, Barbour SL. A study of hysteresis models for soil-water characteristic curves. *Canadian Geotechnical Journal*. 2005; 42(6): 1548-1568.

Richards B. Measurement of free energy of soil moisture by the psychrometric technique, using thermistors. In: *Moisture Equilibria and Moisture Changes in Soils Beneath Covered Areas, A Symposium-in-print* (Australia). Butterworths. 1965; 35–46.

Ross B. The diversion capacity of capillary barriers. *Water Resources Research*. 1990; 26(10):2625–2629.

Rudiyanto, Sakai M, van Genuchten MT, Alazba AA, Setiawan BI, Minasny B. A complete soil hydraulic model accounting for capillary and adsorptive water retention, capillary and film conductivity, and hysteresis. *Water Resources Research*. 2015; 51(11):8757–8772.

Scarfone R. *Modelling the hydraulic behaviour of unsaturated soils and application to the numerical and experimental study of capillary barrier systems*. PhD thesis, University of Glasgow. 2020.

Scarfone R, Wheeler SJ, Lloret-Cabot M. A conceptual hydraulic conductivity model for unsaturated soils at low degree of saturation and application to the study of capillary barrier systems. *Journal of Geotechnical and Geoenvironmental Engineering*. 2020; 146(10):04020106.

Schelle H, Heise L, Jänicke K, Durner W. Water retention characteristics of soils over the whole moisture range: a comparison of laboratory methods. *European journal of soil science*. 2013; 64(6):814–821.

Scott P, Farquhar G, Kouwen N. Hysteretic effects on net infiltration. In: *Advances in infiltration*. American Society of Agricultural Engineers, St. Joseph, Mich., 1983: 163–170.

Servizio metereologico Aeronautica Militare. http://www.meteoam.it/; Last accessed 05/02/2018.

Stonestrom DA, Rubin J. Water content dependence of trapped air in two soils. *Water Resources Research*. 1989; 25(9): 1947-1958.

Stormont JC, Anderson CE. Capillary barrier effect from underlying coarser soil layer. *Journal of Geotechnical and Geoenvironmental Engineering*. 1999; 125(8):641-648.

Stormont JC, Morris CE. Method to estimate water storage capacity of capillary barriers. *Journal of Geotechnical and Geoenvironmental Engineering*. 1998; 124(4), 297-302.

Tami D, Rahardjo H, Leong EC, Fredlund DG. Design and laboratory verification of a physical model of sloping capillary barrier. *Canadian Geotechnical Journal*. 2004; 41(5):814–830.

Topp GC, Miller E. Hysteretic moisture characteristics and hydraulic conductivities for glass-bead media 1. *Soil Science Society of America Journal*. 1966; 30(2):156–162.

Vachaud G, Thony JL. Hysteresis during infiltration and redistribution in a soil column at different initial water contents. *Water Resources Research*. 1971; 7(1):111–127.

van Genuchten MT. A closed-form equation for predicting the hydraulic conductivity of unsaturated soils. *Soil science society of America journal*. 1980; 44(5):892-898.

Wheeler SJ, Sharma R, Buisson M. Coupling of hydraulic hysteresis and stress–strain behaviour in unsaturated soils. *Géotechnique*. 2003; 53(1):41–54.

Zhan TL, Ng CW. Analytical analysis of rainfall infiltration mechanism in unsaturated soils. *International Journal of Geomechanics*. 2004; 4(4):273–284.

Zhang L, Fredlund D, Zhang L, Tang W. Numerical study of soil conditions under which matric suction can be maintained. *Canadian Geotechnical Journal*. 2004; 41(4): 569–582.

Zhang Q, Werner AD, Aviyanto RF, Hutson JL. Influence of soil moisture hysteresis on the functioning of capillary barriers. *Hydrological Processes: An International Journal*. 2009; 23(9):1369–1375.

Zhou AN, Sheng D, Sloan SW, Gens A. Interpretation of unsaturated soil behaviour in the stress–saturation space, i: volume change and water retention behaviour. *Computers and Geotechnics*. 2012; 43:178–187.

Tables

Table 1. Hysteretic modVG SWRC model parameter values for Tottori sand and Wray sand

Soil	θ_{ls}	Drying curves					Wetting curves				
		$S_{ls,d}$	ξ_d	$P_{0,d}$	n_d	γ_d	$S_{ls,w}$	ξ_w	$P_{0,w}$	n_w	γ_w
	[-]	[-]	[-]	[kPa]	[-]	[-]	[-]	[-]	[kPa]	[-]	[-]
Tottori sand	0.374	1.00	0.0107	2.90	7.77	6.25	0.92	0.0107	1.73	5.45	5.41
Wray sand	0.301	1.00	0.0281	3.166	9.45	6.34	1.00	0.0277	1.834	5.46	5.30

Table 2. Hysteretic modVG-modM+LF SWRC and SHCC model parameter values for aggregated glass beads

	Primary drying			Main drying			Main wetting								
θ_{ls}	$S_{ls,d}$	$P_{0,d}$	n	$S_{ls,d}$	$P_{0,d}$	n	$S_{ls,w}$	$P_{0,w}$	n	ξ	γ_d	γ_w	k_{ls}	$S_{l,BWC/BWD}$	C^{Film}
[-]	[-]	[kPa]	[-]	[-]	[kPa]	[-]	[-]	[kPa]	[-]	[-]	[-]	[-]	[m/s]	[-]	[$ms^{-1}kPa^{1.5}$]
0.609	1.00	4.03	10.53	0.90	3.95	9.61	0.90	2.46	6.46	0.0131	7.85	4.20	3.3E-4	0.15	4.6E-9

Table 3. Constitutive laws and parameters used in the FE analyses

Soil water retention curve, SWRC	$S_{le,d} = \left\{1+\left[\dfrac{\left(s^{\gamma_d}-A_d\right)^{1/\gamma_d}}{P_{0d}}\right]^{n_d}\right\}^{-m_d}$	**C.L. H**	P_{0d}=1.65E-4 MPa, P_{0w}=4.60E-5 MPa, m_d=m_w=0.604, ξ_d=ξ_w=1.82E-3, S_{lsd}=S_{lsw}=1, γ_d=γ_w=4, s_{dry}=1 GPa
		C.L. D	P_{0d}=1.65E-4 MPa, m_d=0.604, ξ_d=1.82E-3, S_{lsd}=1, γ_d=4, s_{dry}=1 GPa
	$S_{le,w} = \left\{1+\left[\dfrac{\left(s^{-\gamma_w}-A_w\right)^{-1/\gamma_w}}{P_{0w}}\right]^{n_w}\right\}^{-m_w}$	**C.L. W**	P_{0w}=4.60E-5 MPa, m_w=0.604, ξ_w=1.82E-3, S_{lsw}=1, γ_w=4, s_{dry}=1 GPa
	$S_{l,d} = \xi_d \ln\left(\dfrac{s_{dry}}{s}\right)+\left[S_{ls,d}-\xi_d \ln\left(\dfrac{s_{dry}}{s}\right)\right]\cdot S_{le,d}$	**F.L. H**	P_{0d}=5.85E-3 MPa, P_{0w}=3.34E-3 MPa, m_w=m_d=0.812, ξ_d=ξ_w=1.47E-3, S_{lsd}=S_{lsw}=1, γ_d=γ_w=9, s_{dry}=1 GPa
	$S_{l,w} = \xi_w \ln\left(\dfrac{s_{dry}}{s}\right)+\left[S_{ls,w}-\xi_w \ln\left(\dfrac{s_{dry}}{s}\right)\right]\cdot S_{le,w}$	**F.L. D**	P_{0d}=5.85E-3 MPa, m_d=0.812, ξ_d=1.47E-3, S_{lsd}=1, γ_d=9, s_{dry}=1 GPa
		F.L. W	P_{0w}=3.34E-3 MPa, m_w=0.812, ξ_w=1.47E-3, S_{lsw}=1, γ_w=9, s_{dry}=1 GPa
Soil hydraulic conductivity curve, SHCC	$k_l = k_{ls}\cdot\sqrt{S_l^{\,C}}\left[1-\left(1-\left(S_l^{\,B}\right)^{1/m}\right)^m\right]^2 + C^{Film}\cdot\left(a^{Film}+s\right)^{-1.5}$	**C.L.**	k_{ls}=7.6E-2 m/s, $S_{l,BWC}$=$S_{l,BWD}$=0.15, $S_{l,BWE}$=$S_{l,BWEX}$=0.15, a^{Film}=5E-5 MPa, C^{Film}=1.702E-14 MPa$^{1.5}$ms^{-1}
	$S_l^{\,C} = \dfrac{S_l - S_{l,BWC/BWD}}{S_{ls}-S_{l,BWC/BWD}}$ $S_l^{\,B} = \dfrac{S_l - S_{l,BWE/BWEX}}{S_{ls}-S_{l,BWE/BWEX}}$	**F.L.**	k_{ls}=1.4E-4 m/s, $S_{l,BWC}$=$S_{l,BWD}$=0.15, $_{l,BWE}$=$S_{l,BWEX}$=0.15, a^{Film}=1E-4 MPa, C^{Film}=4.379E-13 MPa$^{1.5}$ms^{-1}
Diffusion of water vapour in the gas phase (Fick's Law)*	$\mathbf{i_g}^{\mathbf{w}} = -\left(\tau\phi\rho_g S_g D_g^{\,w}\mathbf{I}\right)\nabla\omega_g^{\,w}$	**C.L.**	ϕ=0.382, τ=1, D=5.9E-6 m^{2}Pas^{-1}K^{-n}, n=2.3
	$D_g^{\,w} = D\left[\dfrac{\left(273.15\mathrm{K}+T\right)^n}{p_g}\right]$	**F.L.**	ϕ=0.382, τ=1, D=5.9E-6 m^{2}Pas^{-1}K^{-n}, n=2.3
Conductive flux of heat (Fourier's Law)*	$\mathbf{i_c} = -\lambda\nabla T$ $\lambda = \lambda_{sat}\sqrt{S_l}+\lambda_{dry}\left(1-\sqrt{S_l}\right)$	**C.L.**	λ_{solid}=7.7 Wm^{-1}K^{-1}, λ_{gas}=0.02619 Wm^{-1}K^{-1}, λ_{liquid}=0.591 Wm^{-1}K^{-1}
	$\lambda_{dry} = \lambda_{solid}^{(1-\phi)}\lambda_{gas}^{\ \phi}$ $\lambda_{sat} = \lambda_{solid}^{(1-\phi)}\lambda_{liq}^{\ \phi}$	**F.L.**	λ_{solid}=7.7 Wm^{-1}K^{-1}, λ_{gas}=0.02619 Wm^{-1}K^{-1}, λ_{liquid}=0.591 Wm^{-1}K^{-1}

* Only used in numerical analyses of stage 2

SWRC (subscript d for drying paths, subscript w for wetting paths): S_l=(liquid) degree of satuation; S_{le}=effective (liquid) degree of saturation; λ, P_0 [MPa], γ=parameters controlling the shape of the SWRC; ξ: parameter controlling the residual degree of saturation function; s_{dry} [MPa]=suction corresponding to complete dryness; A=function of the last reversal point, controls the position of the scanning curve (A=0 for main wetting or main drying curves). **SHCC**: k_{ls}=saturated hydraulic conductivity; C^{film} [ms^{-1}MPa$^{1.5}$], a^{film} [MPa]= parameters governing the liquid film component of the hydraulic conductivity; $S_{l,BWD}$= bulk water discontinuity value of the degree of saturation; $S_{l,BWEX}$= bulk water exclusion value of the degree of saturation; $S_{l,BWC}$= bulk water continuity value of the degree of saturation; $S_{l,BWE}$= bulk water entry value of the degree of saturation. **Fick's Law**: $\mathbf{i^w_g}$ [kg m^{-3} s^{-1}]=diffusive water flow in the gas phase; τ=tortuosity; ϕ=porosity; ρ_g [kg/m^3]=gas density; S_g=gas degree of saturation (S_g=1-S_l); D^w_g [m^2/s]=diffusion coefficient of water in the gas phase; ω^w_g [kg of water per kg of gas]=water mass fraction in the gas phase; D [m^2/s], n =parameters of the model; T [K]=temperature. **Fourier's Law**: $\mathbf{i_c}$ [W/m^2]=conductive heat flux; λ [W m^{-1} K^{-1}]=thermal conductivity; λ_{solid} [W m^{-1} K^{-1}]=thermal conductivity of the solid phase; λ_{gas} [W m^{-1} K^{-1}]=thermal conductivity of the gas phase; λ_{liq} [W m^{-1} K^{-1}]=thermal conductivity of the liquid phase.

Table 4. Atmospheric parameters used for numerical analyses during stage 2

z_0 [m]	z_a [m]	ψ [-]	ρ_{ga} [kg/m^3]	T_a [°C]	p_{ga} [MPa]	RH_a [-]	R_n [Jm^{-2}s^{-1}]	v_a [m/s]
0.001	2	1	1.1883	25.5	0.1	0.65	325	3.14

Figures

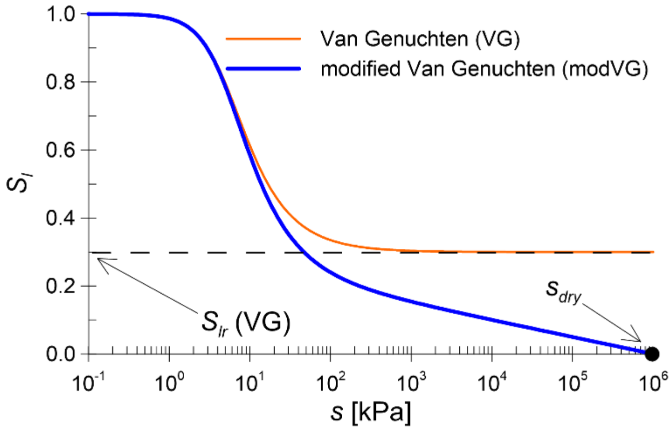

Figure 1. Qualitative comparison between SWRCs predicted by the VG and the modVG models

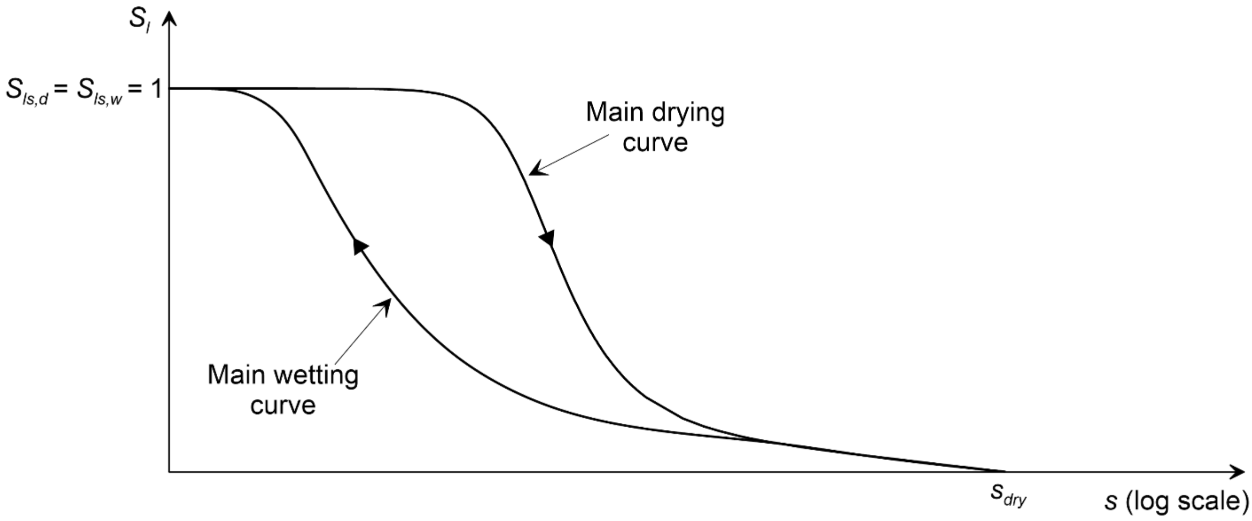

Figure 2. Typical main drying and main wetting SWRCs predicted by the modVG model

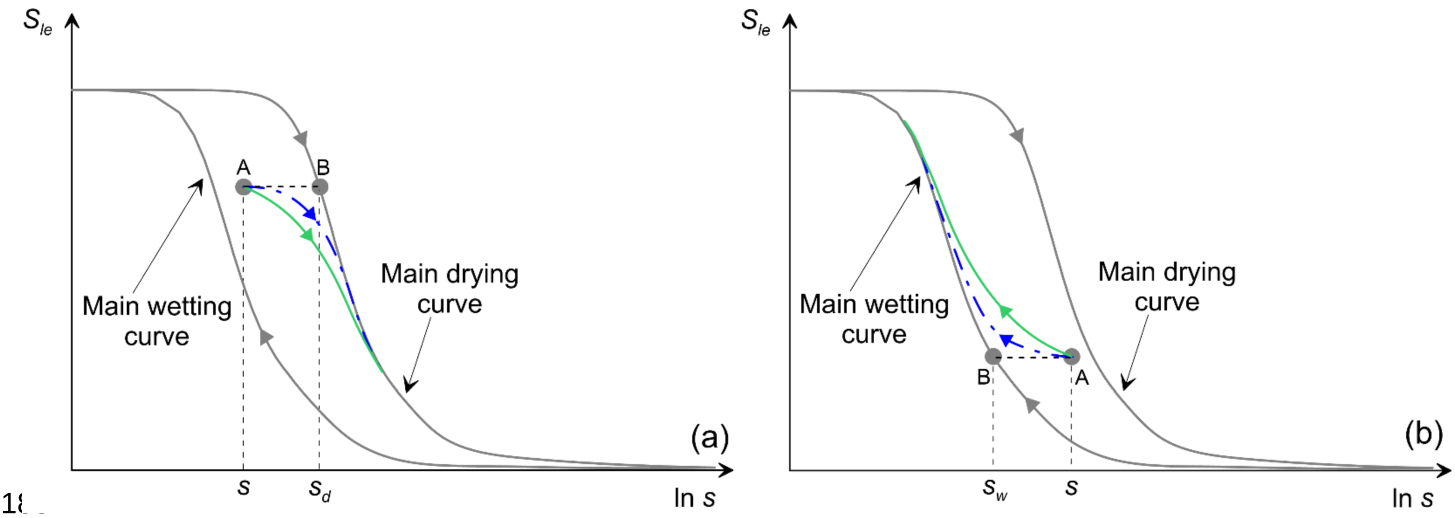

Figure 3. Water retention (a) drying scanning curve and (b) wetting scanning curve, shown in S_{le} : ln$s$ plots

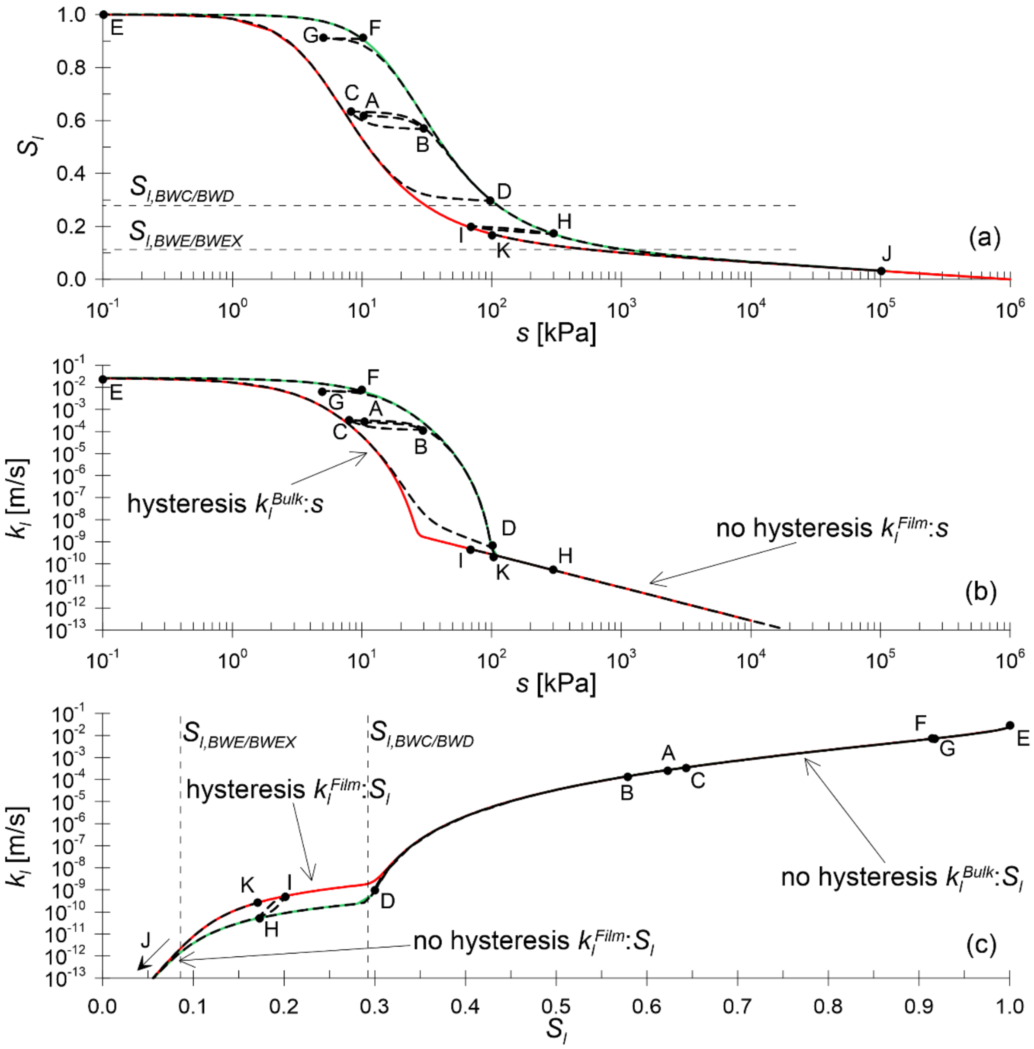

Figure 4. Performance of the hysteretic hydraulic model: (a) SWRC, (b) SHCC plotted against suction s and (c) SHCC plotted against degree of saturation S_l

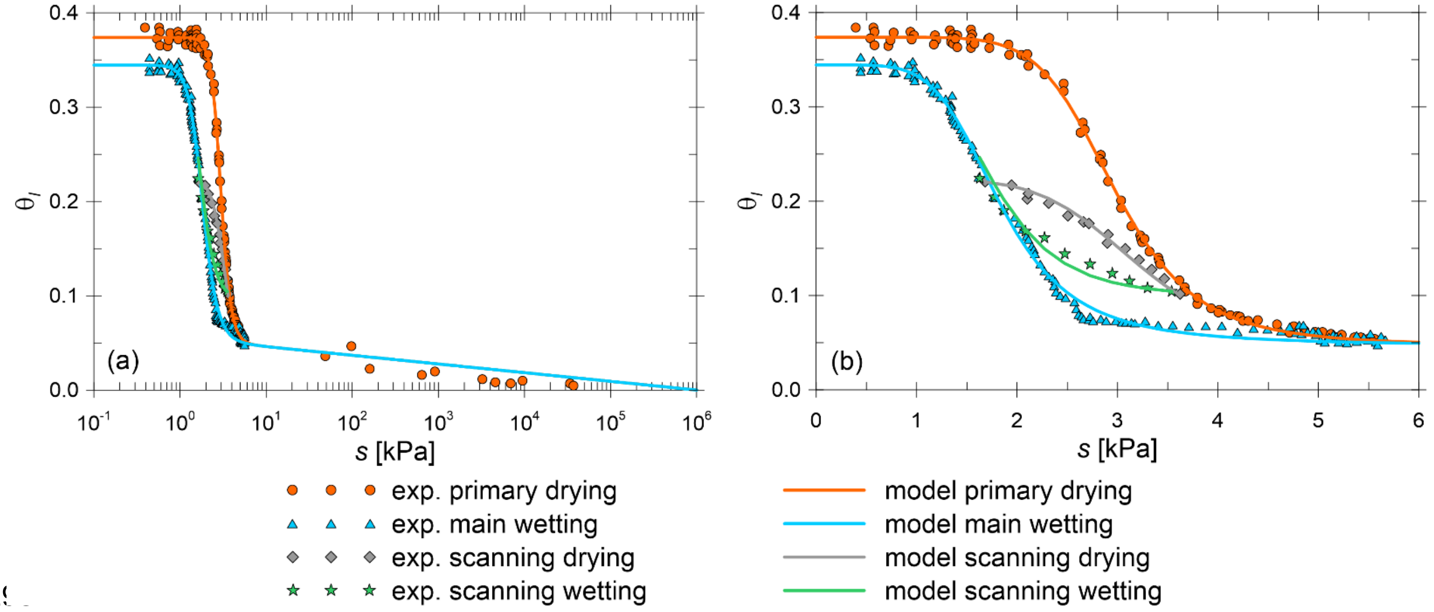

Figure 5. Comparison between experimental SWRC data for Tottori sand (Rudiyanto et al., 2015) and hysteretic modVG model: (a) full range of suction; (b) zoom at low suction

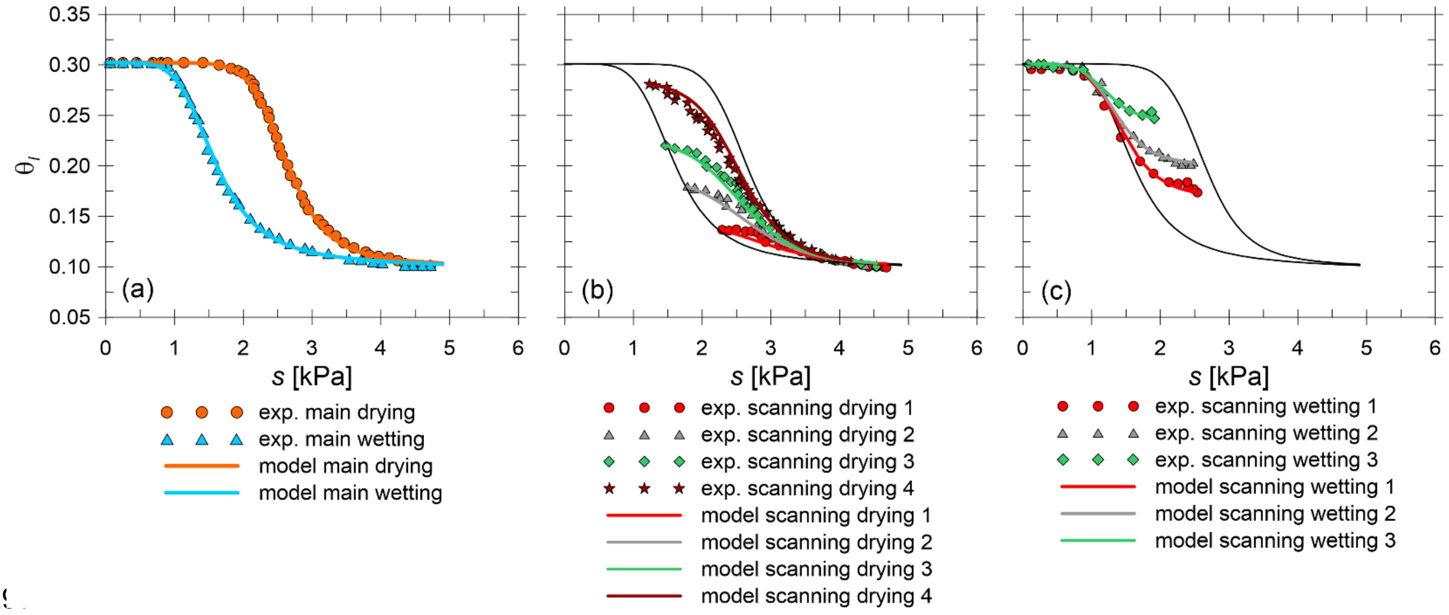

Figure 6. Comparison between experimental SWRC data for Wray sand (Gillham et al., 1976) and hysteretic modVG model: (a) main drying and main wetting curves, (b) scanning drying curves, (c) scanning wetting curves

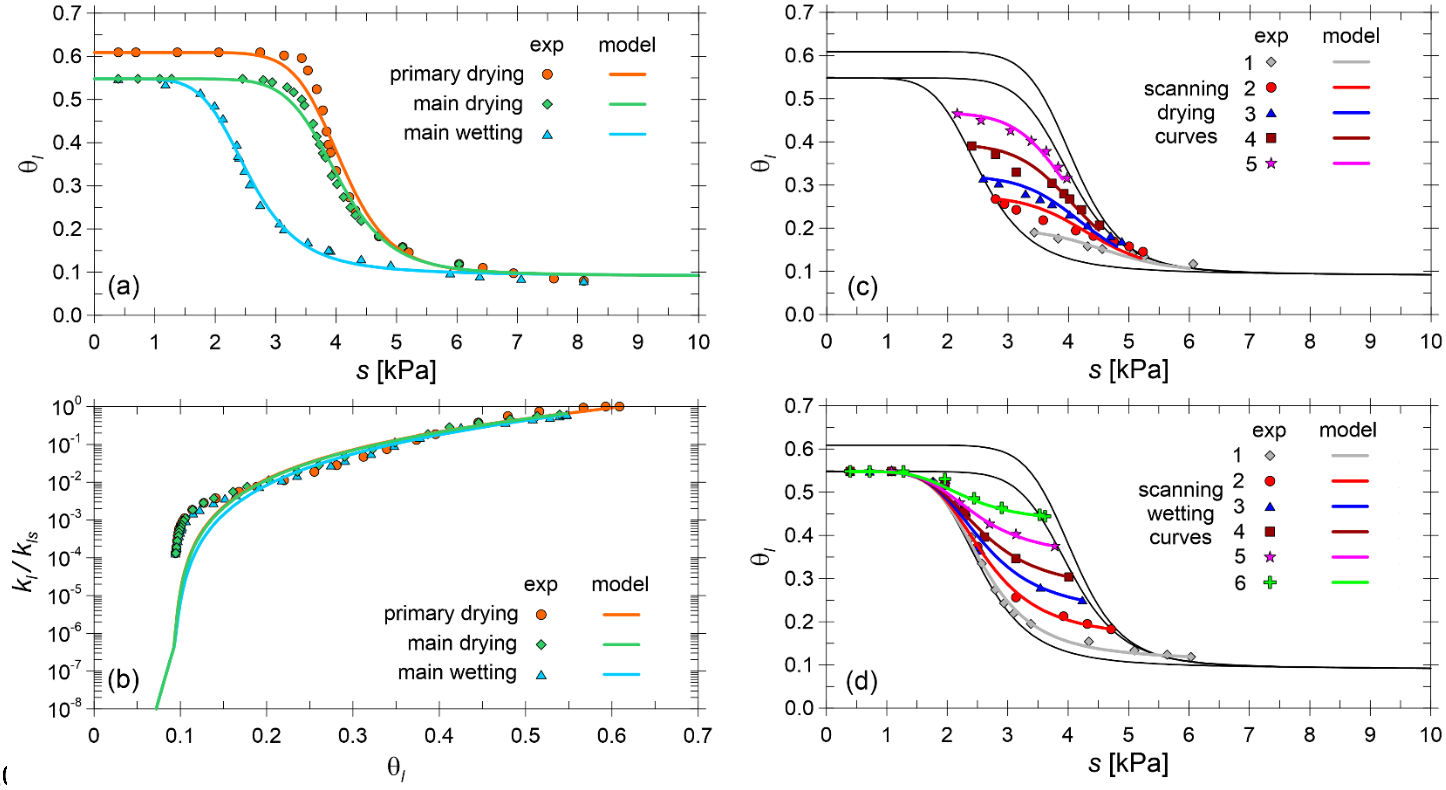

Figure 7. Comparison between experimental data for aggregated glass beads (Topp and Miller, 1966) and hysteretic modVG-modM+LF model: primary drying curve, main drying curve and main wetting curve ((a) θ_l:s and (b) k_{lr}:θ_l), (c) scanning drying curves (θ_l:s) and (d) scanning wetting curves (θ_l:s)

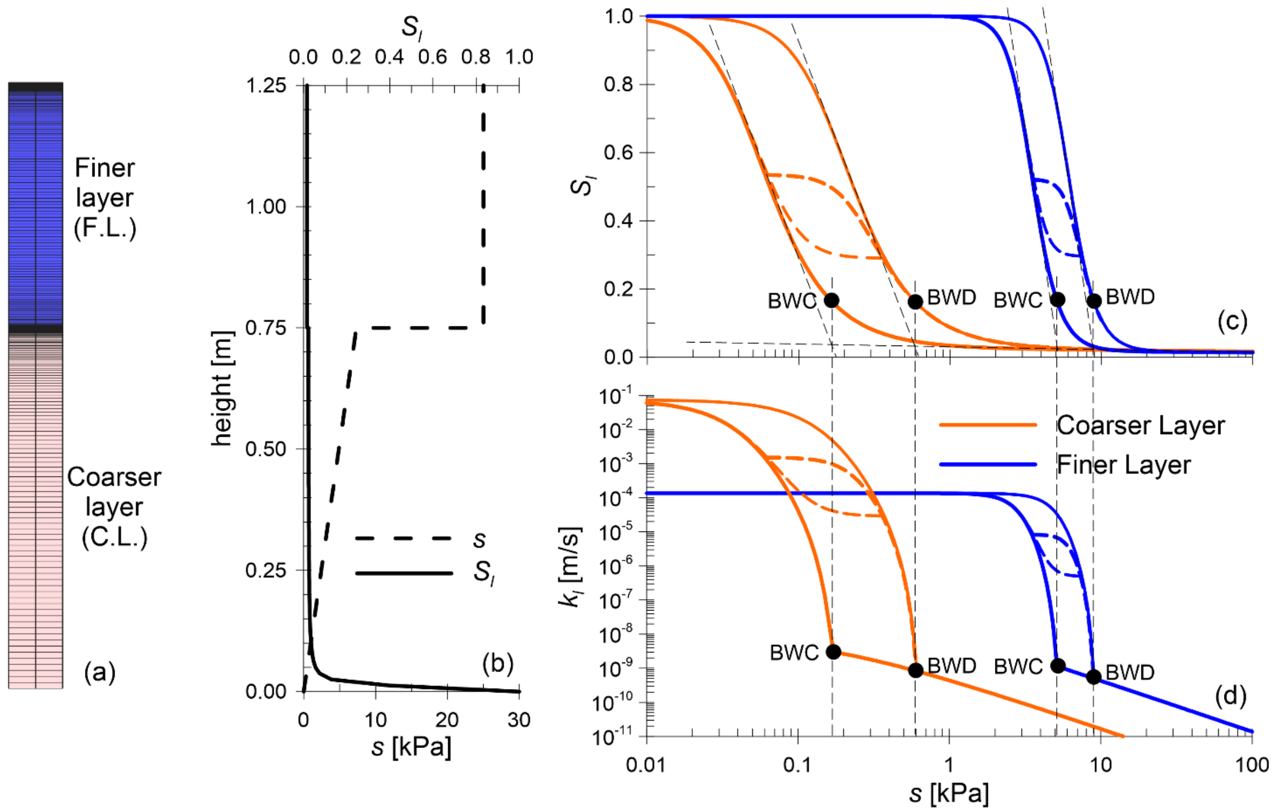

Figure 8. Properties of the numerical model: (a) mesh, (b) initial conditions for stage 1a and 2, (c) SWRC models and (d) SHCC models

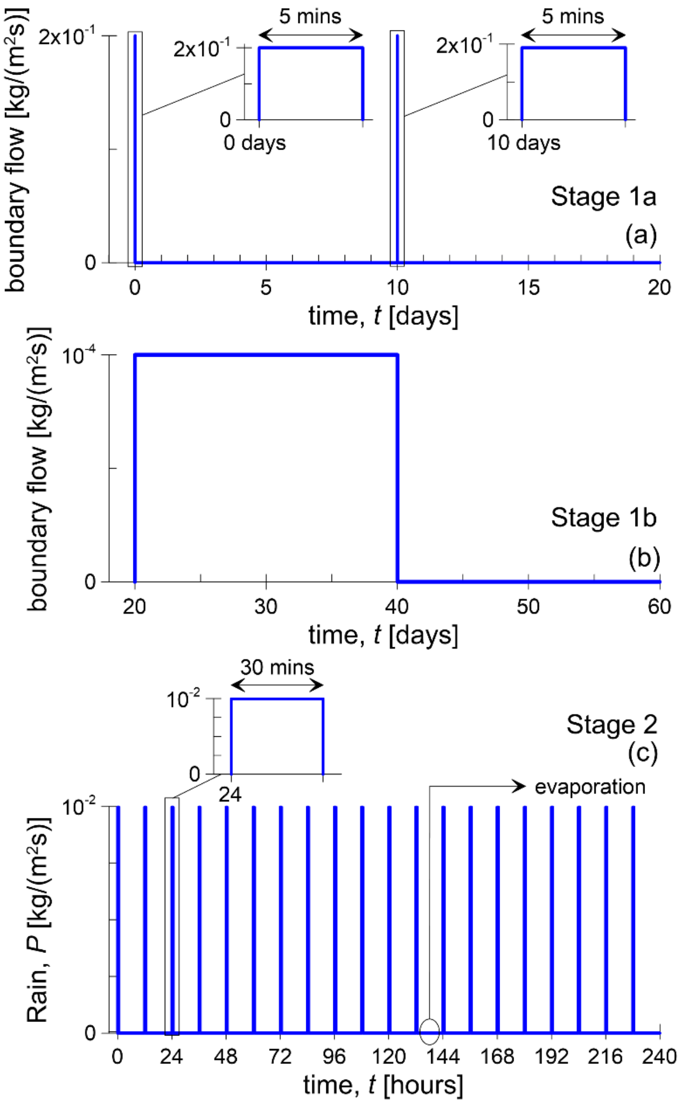

Figure 9. Time history of the liquid water flow applied at the top boundary during (a) stage 1a, (b) stage 1b and (c) stage 2

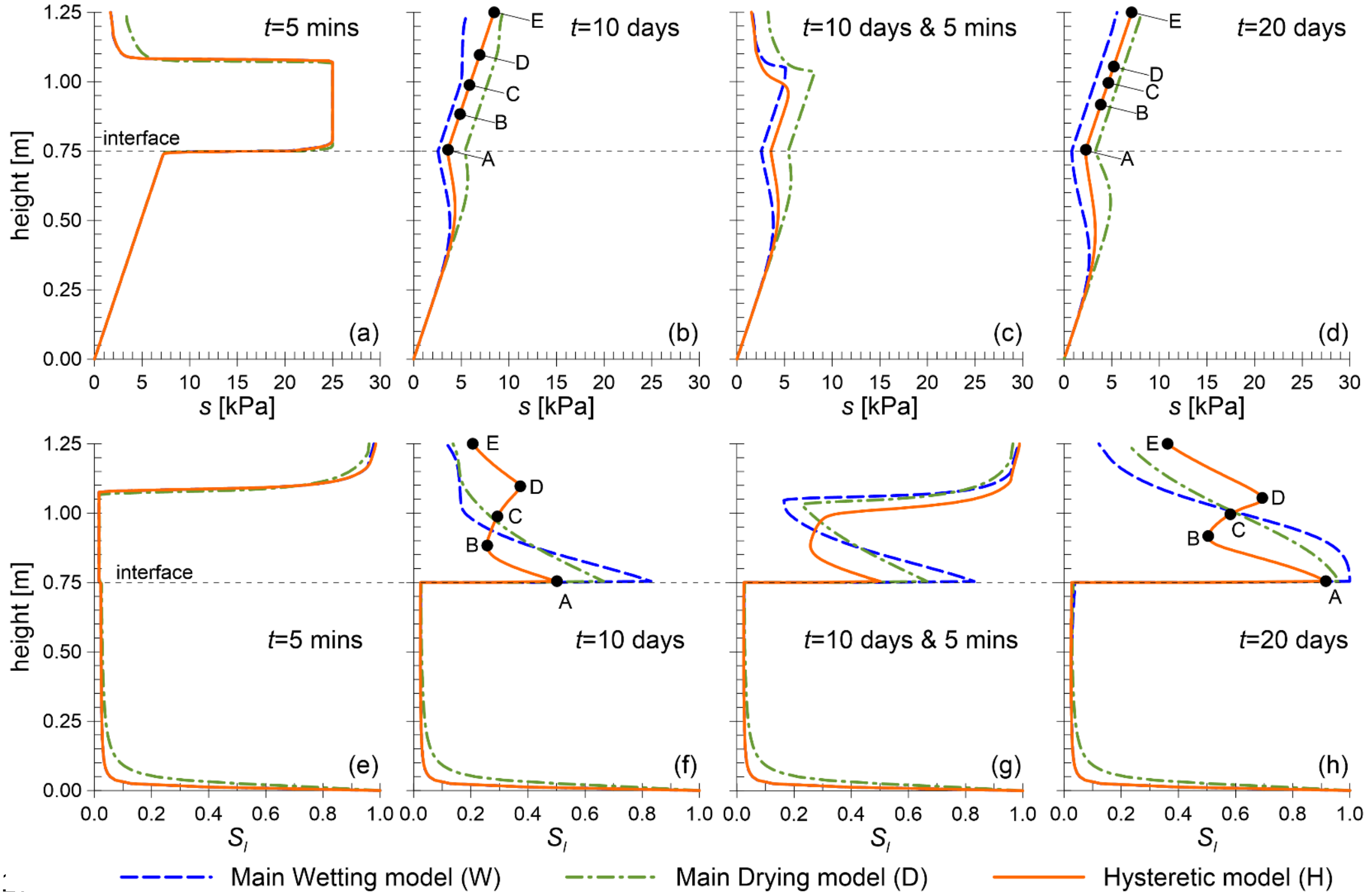

Figure 10. Stage 1a: suction (a-d) and degree of saturation (e-h) profiles at different times

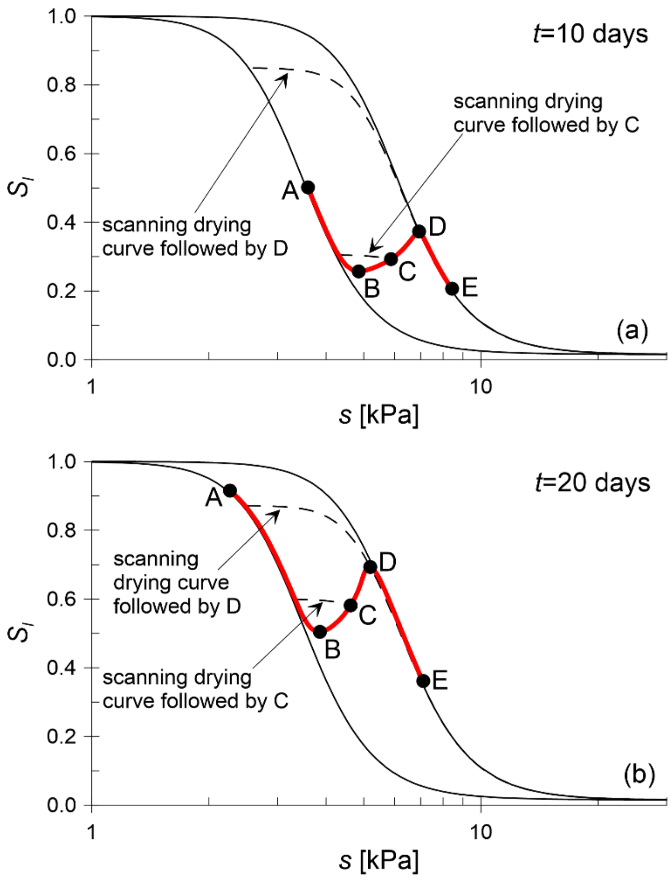

Figure 11. Stage 1a: interpretation of the s:S_l profiles in the finer layer at times (a) t=10 days and (b) t=20 days

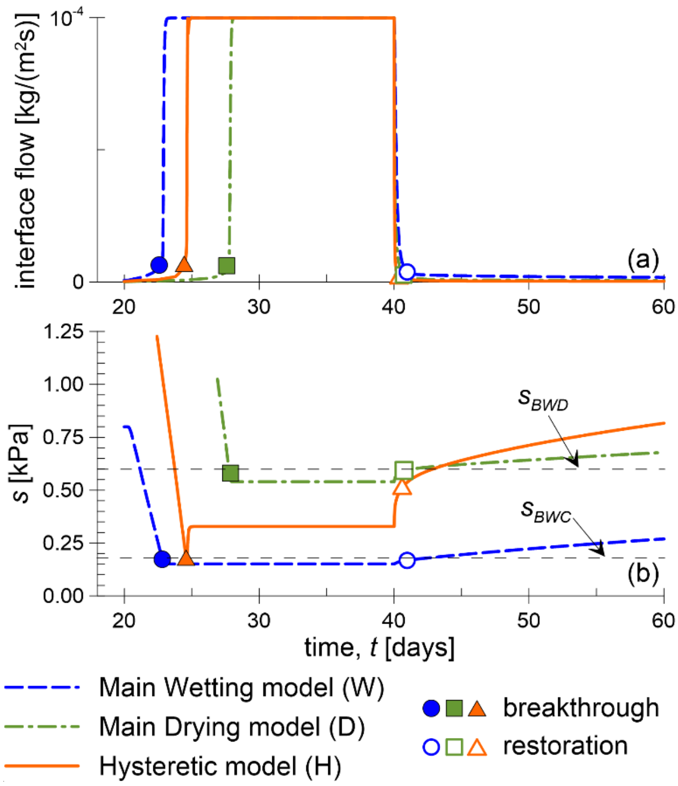

Figure 12. Stage 1b: time histories of (a) liquid flow at the interface and (b) suction at the interface

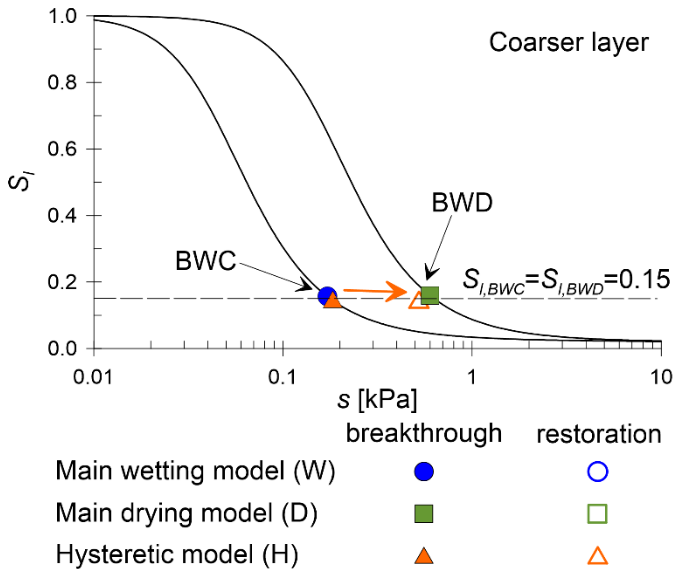

Figure 13. Stage 1b: interpretation of the s:S_l points in the coarser layer at the interface at breakthrough and restoration

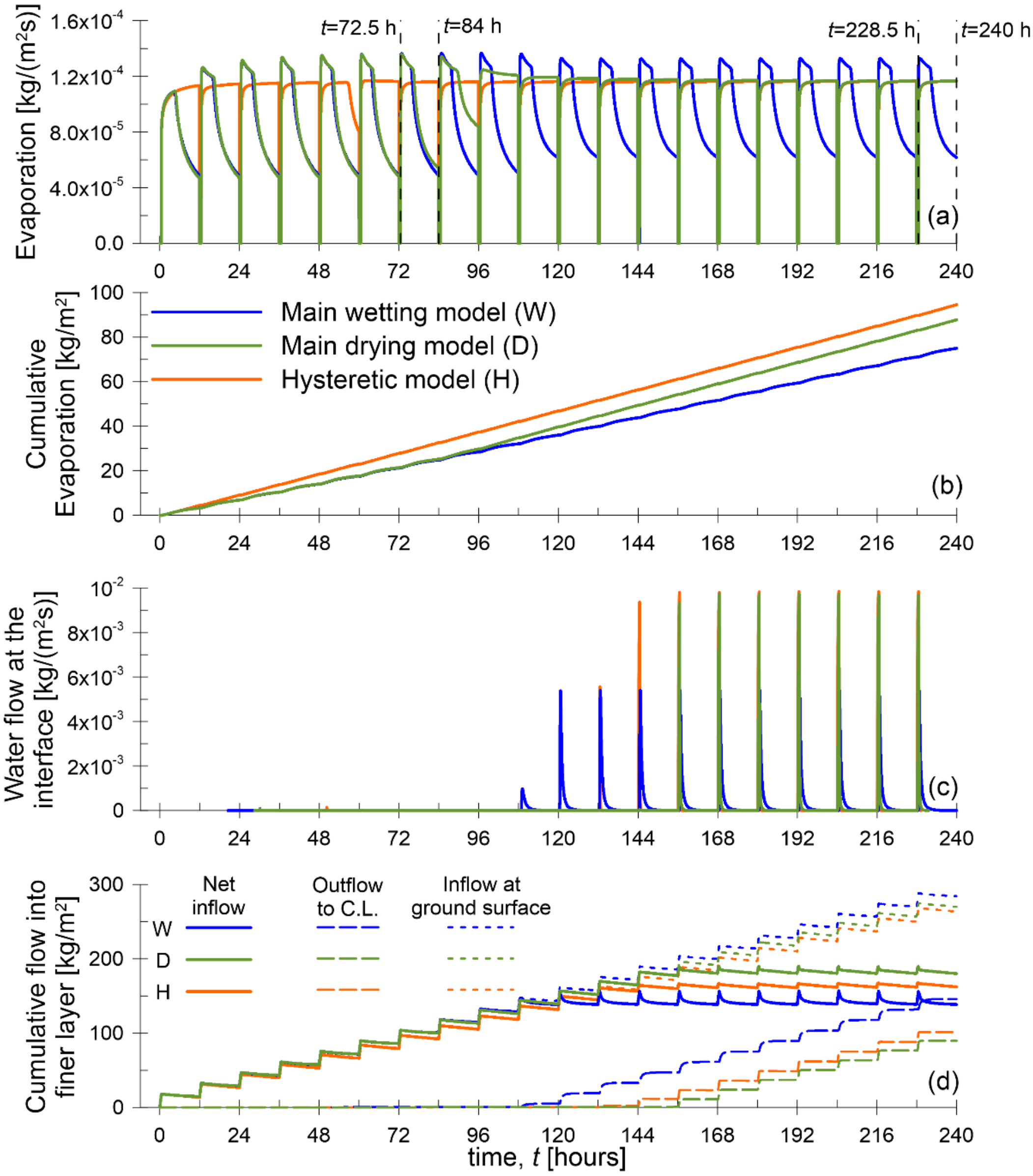

Figure 14. Stage 2: time histories of (a) evaporation rate from the ground surface, (b) cumulative evaporation, (c) water flow rate across the interface, (d) cumulative inflow and outflow to/from the finer layer

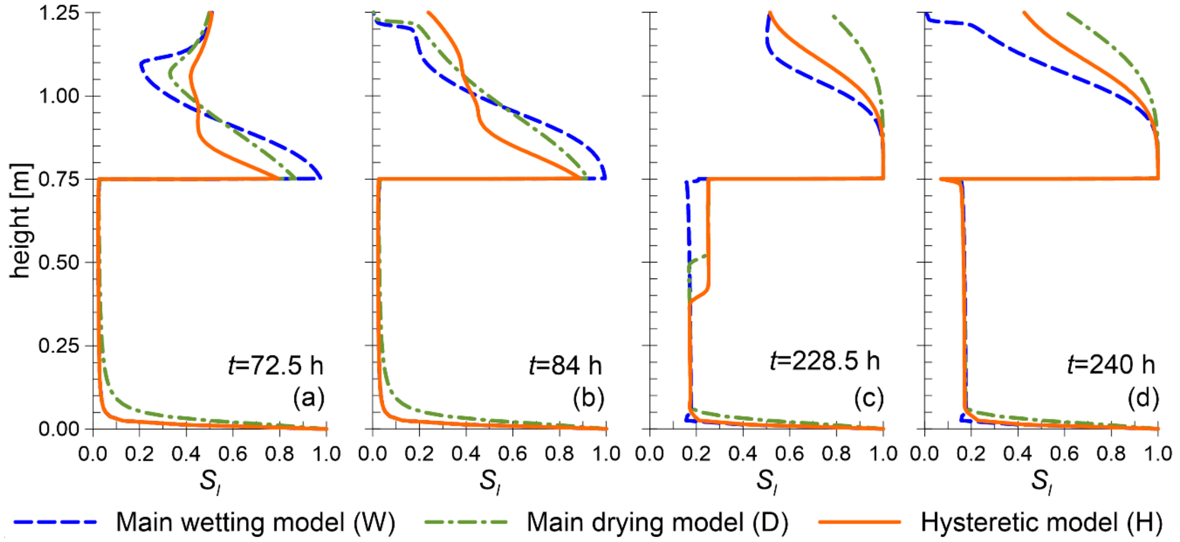

Figure 15. Stage 2: degree of saturation profiles at different times: (a) *t*=72.5 h, (b) *t*=84 h, (c) *t*=228.5 h and (d) *t*=240 h